In the formation of **5**, alkyne coupling did occur at the less crowded, unsubstituted carbon atoms, but unfortunately, the reaction was accompanied by degradation of the cluster.

Compounds **3-5** also contain COD ligands. It seems likely that these compounds should permit further study of the heteronuclear iron-platinum center. Further studies are in progress.

(21) Riley, P. E.; Davis, R. E. *Acta Crystallogr.* 1975, *B31*, 2928.

Acknowledgment. This research was supported by the National Science Foundation under Grant CHE-8919786. We wish to thank Professor C. Mealli for making the results of his studies available to us prior to publication.

Supplementary Material Available: Tables of hydrogen atom coordinates for **2** and **5**, hydrogen and ring carbon coordinates for **4**, and anisotropic thermal parameters for **1**, **2**, **4**, and **5** (16 pages); tables of structure factor amplitudes for **1**, **2**, **4**, and **5** (69 pages). Ordering information is given on any current masthead page.

Synthetic, Structural, and Bonding Studies of Phosphido-Bridged Early-Late Transition-Metal Heterobimetallic Complexes

R. Thomas Baker* and William C. Fultz

Central Research and Development Department,† Experimental Station, E. I. du Pont de Nemours and Co., Wilmington, Delaware 19880-0328

Todd B. Marder* and Ian D. Williams*

Guelph-Waterloo Centre for Graduate Work in Chemistry, Department of Chemistry, University of Waterloo, Waterloo, Ontario, Canada N2L 3G1

Received February 7, 1990

The mononuclear terminal phosphide complexes $Cp_2M(PR_2)_2$ (M = Zr, Hf; R = Et, Ph, Cy) are shown to act as chelating bis(phosphine) ligands to Ni, Pd, and Pt (M') in compounds of the form $Cp_2M(\mu\text{-}PR_2)_2M'L_n$ (n = 1, 2) and $\{Cp_2M(\mu\text{-}PR_2)_2\}_2M'$. Reaction of $Cp_2M(PEt_2)_2$ with $Ni(1,5\text{-}COD)_2$ yields either $Cp_2M(\mu\text{-}PEt_2)_2Ni(1,5\text{-}COD)$ or $\{Cp_2M(\mu\text{-}PEt_2)_2\}_2Ni$ depending on the stoichiometry employed. Analogous reactions with $Pd(PPh_3)_4$ and $Pt(PPh_3)_3$ yield mixtures of $Cp_2M(\mu\text{-}PEt_2)_2M'(PPh_3)$ and $\{Cp_2M(\mu\text{-}PEt_2)_2\}_2M'$ (M' = Pd, Pt) when the M/M' ratio is <2. With bulkier substituents, $Cp_2M(PR_2)_2$ (R = Ph, Cy) react with $Pt(1,5\text{-}COD)_2$ and $CpPd(\eta\text{-}2\text{-}Me\text{-}allyl)$ in the presence of phosphines and phosphites yielding only $Cp_2M(\mu\text{-}PR_2)_2M'L$ (L = PR'_3, $P(OR')_3$). The $M'L_2$ complexes $Cp_2M(\mu\text{-}PPh_2)_2M'(DMPE)$ were also prepared. The three classes of compounds were characterized by X-ray crystallography. The structure of $Cp_2Zr(\mu\text{-}PEt_2)_2Ni(\mu\text{-}PEt_2)_2HfCp_2$ ($C2/c$, Z = 8, a = 34.823 (4), b = 10.991 (2), c = 21.606 (3) Å, β = 105.65 (1)°) consists of two 16-e⁻ d^0 metal centers coupled to a pseudotetrahedral 18-e⁻ d^{10} Ni center by PEt_2 bridges. The MP_2Ni rings are nearly planar with an average M···Ni separation of 3.027 (1) Å. The structure of $Cp_2Hf(\mu\text{-}PPh_2)_2Pd(PPh_3)$ ($C2/c$, Z = 8, a = 27.701 (8), b = 10.654 (5), c = 30.330 (11) Å, β = 103.16 (5)°) consists of edge-shared, 16-e⁻ pseudotetrahedral Hf(IV) and trigonal planar Pd(0) centers with a puckered HfP_2Pd ring and a Hf···Pd separation of 2.896 (1) Å. In the structure of $Cp_2Hf(\mu\text{-}PPh_2)_2Pd(DMPE)$ ($C2/c$, Z = 8, a = 25.361 (12), b = 19.584 (5), c = 18.814 (13) Å, β = 126.15 (5)°) the 16-e⁻ Hf(IV) and 18-e⁻ Pd(0) centers are pseudotetrahedral, the HfP_2Pd ring is puckered and the Hf···Pd separation is 2.983 (1) Å. Extended Hückel molecular orbital calculations performed on the model complexes $Cp_2Zr(\mu\text{-}PH_2)_2M'L_n$ ($M'L_n$ = $Pt(PH_3)$, Pt(DMPE), $Rh(\eta^5\text{-indenyl})$, $Ni(\mu\text{-}PH_2)_2ZrCp_2$, and $Mo(CO)_4$) indicate the presence of M' → Zr donor-acceptor metal-metal bonds that become weaker along the series. The calculations also predict low barriers to MP_2M' ring inversion for the Pt complexes, consistent with low-temperature ^1H and ^{31}P NMR spectroscopic observations.

Introduction

Diorganophosphide $(PR_2)^-$ ligands have been widely used as bridging groups in transition-metal chemistry[1] due to the ease with which steric and electronic factors can be tuned. In bis$(PR_2)^-$-bridged complexes that have been structurally characterized,[2,3] the M-P-M' angles and M-M' distances range from 54 to 104° and 2.21 (multiple M-M bond) to 3.70 Å (M-M nonbonding), respectively, also indicating the flexibility of $(\mu\text{-}PR_2)$ groups.

As part of an extensive study of early-transition-metal complexes containing terminal $(PR_2)^-$ ligands,[4-6] we have prepared and structurally characterized[4a] $Cp_2Hf(PEt_2)_2$. This contains both planar and pyramidal phosphido groups

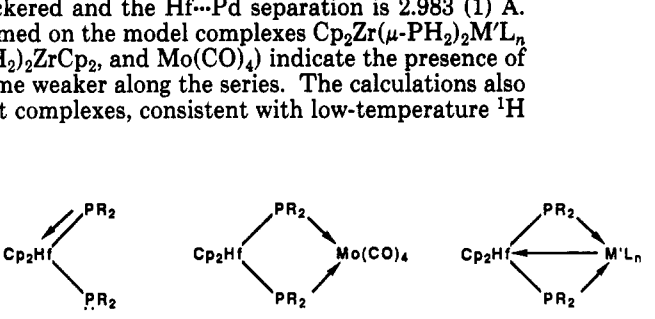

consistent with electronic structure (A) in which the Hf center is saturated. Subsequently, we demonstrated[7] the ability of $Cp_2Hf(PEt_2)_2$ to function as a bidentate phosphine ligand in $Cp_2Hf(\mu\text{-}PEt_2)_2Mo(CO)_4$ in which the Hf-Mo distance is 3.400 (1) Å. Spectroscopic properties of the heterobimetallic complex suggest that there is no significant perturbation of the $Mo(CO)_4$ unit due to interaction with the Hf, which is now electronically unsat-

† Contribution No. 4832.

0276-7333/90/2309-2357$02.50/0

urated (B). The 16-electron Hf center could however serve as a Lewis acid to an electron-rich late-metal fragment (C).

We have explored this possibility and report herein (1) the binding of $Cp_2M(PR_2)_2$ moieties (M = Zr, Hf) to group 10 {M'}, {M'L}, and {M'L_2} fragments (L = phosphine, phosphite), (2) the molecular structures of a representative example of each of these, (3) extended Hückel molecular orbital calculations on these complexes and on d^8-[M'L_3] and d^6-[M'L_4] analogues, and (4) experimental observations that indicate that the presence of a donor–acceptor M' → M bond in the $Cp_2M(\mu\text{-}PR_2)_2M'(PR_3)$ complexes significantly affects the reactivity at the group 10 metal center. Some of this work has been communicated previously[8,9] and related synthetic studies have been reported[10] by Gelmini and Stephan.

Experimental Section

Materials and Characteriztion. All operations were conducted in a Vacuum Atmospheres glovebox with continuous nitrogen flush. Solvents were purified by standard techniques and distilled from sodium or potassium benzophenone ketyl. Literature methods were used to prepare $Pd(PPh_3)_4$,[11] (η-C_5H_5)Pd(η-2-Me-allyl),[12] Pt(1,5-COD)$_2$,[13] $Pt(PPh_3)_3$,[14] (η-$C_5H_5)_2M(PR_2)_2$ (M = Zr, Hf; R = Et, Ph, cyclohexyl),[4a] and (η-$C_5H_5)_2$Hf[PhP$(CH_2)_3$PPh].[4a] Tertiary phosphorus ligands and Ni(1,5-COD)$_2$ (Strem), MeI, CNBu^t, benzaldehyde, paraformaldehyde, NH_4PF_6, MeC(O)Br (Aldrich), research purity H_2, CO, and ethylene (Matheson) were used as received. NMR spectra were recorded on a Nicolet NMC-300-WB (121-MHz ^{31}P) spectrometer, and ^{31}P NMR chemical shifts are positive downfield from external 85% H_3PO_4. IR spectra were recorded as Nujol mulls between NaCl or CsI plates on a Perkin-Elmer 983 spectrometer. Elemental analyses were performed by Pascher Mikroanalytisches Labor, Remagen, West Germany. Complete elemental analyses (C, H, P, M, M') and IR spectroscopic data for isolated complexes are listed in Tables IX and X (supplementary material (see the paragraph at the end of the paper)). ^{1}H and ^{31}P NMR spectroscopic data are listed in Tables I and II.

Synthesis. $Cp_2Zr(\mu\text{-}PEt_2)_2Ni(1,5\text{-}COD)$ (1a). A solution of 200 mg (0.5 mmol) of $Cp_2Zr(PEt_2)_2$ in 10 mL of THF was added dropwise to 138 mg (0.5 mmol) of Ni(1,5-COD)$_2$ suspended in 5 mL of THF. The solution turned orange to red-orange. After stirring for 12 h, the solution was concentrated in vacuo to 5 mL and cooled at −30 °C for 4 h. The resulting orange crystals were filtered off, washed with 5 mL of cold (−30 °C) pentane, and dried in vacuo, yielding 130 mg. A second crop of 30 mg obtained similarly brought the total yield of **1a** to 160 mg (56%). The Hf analogue, **1b**, was prepared similarly by using 244 mg (0.5 mmol) of $Cp_2Hf(PEt_2)_2$ and 138 mg (0.5 mmol) of Ni(1,5-COD)$_2$ to give 228 mg (70%) of orange crystals.

[$Cp_2Zr(\mu\text{-}PEt_2)_2]_2Ni$ (2a). A solution of 400 mg (1.0 mmol) of $Cp_2Zr(PEt_2)_2$ in 5 mL of THF was added dropwise to a suspension of 138 mg (0.5 mmol) of Ni(1,5-COD)$_2$ in 5 mL of THF. The solution turned orange to dark red. Upon standing for 20 h, the resulting dark red crystals were filtered off, washed with 5 mL of cold (−30 °C) pentane, and dried in vacuo, yielding 299 mg (64% based on **2a**·THF). The analogous Hf complex, **2b**, was prepared on the same scale by using 488 mg of $Cp_2Hf(PEt_2)_2$, yielding 356 mg of red crystals (64%).

$Cp_2Zr(\mu\text{-}PEt_2)_2Ni(\mu\text{-}PEt_2)_2HfCp_2$ (2c). A solution of 200 mg (0.5 mmol) of $Cp_2Zr(PEt_2)_2$ in 10 mL of THF was added dropwise to a suspension of 138 mg (0.5 mmol) of Ni(1,5-COD)$_2$ in 5 mL of THF, yielding a red-orange solution of **1a**. After this stirred for 10 min, a solution of 244 mg (0.5 mmol) of $Cp_2Hf(PEt_2)_2$ in 5 mL of THF was added, affording a dark red solution. Upon standing for 10 days, the resulting dark red crystals were filtered off, washed with 5 mL of cold (−30 °C) pentane, and dried in vacuo, yielding 250 mg. A second crop of 124 mg brought the total yield of **2c** to 374 mg (74%).

{$Cp_2Hf[\mu\text{-}PhP(CH_2)_3PPh]$}$_2$Ni (2d). A solution of 303 mg (0.5 mmol) of $Cp_2Hf[PhP(CH_2)_3PPh]\cdot{}^1/_2C_6H_6$ in 20 mL of THF was added to 69 mg (0.26 mmol) of solid Ni(1,5-COD)$_2$. The solution

(1) (a) Hayter, R. G. *J. Am. Chem Soc.* **1962**, *84*, 3046. (b) Green, M. L. H. *Z. Naturforsch.* **1962**, *17b*, 783. (c) Emeleus, H. J.; Grobe, J. *Angew. Chem., Int. Ed. Engl.* **1962**, *1*, 400. (d) Chatt, J.; Davidson, J. M. *J. Chem. Soc.* **1964**, 2433. (e) Hieber, W. *Z. Naturforsch.* **1963**, *18b*, 1132. (f) Issleib, K.; Hackert, H. *Ibid.* **1966**, *21b*, 519. (g) Ellerman, J.; Poersch, E. *Angew. Chem., Intl. Ed. Eng.* **1967**, *6*, 355. (h) Mais, R. H. B.; Owston, P. G.; Thompson, D. T. *J. Chem. Soc. A* **1967**, 1735. (i) Stone, F. G. A. *Ibid.* **1969**, 1881. (j) Yasufuku, K.; Yamazaki, H. *J. Organomet. Chem.* **1971**, *28*, 415. (k) Schunn, R. A. *Inorg. Chem.* **1973**, *12*, 1573. (l) Johannsen, G.; Stelzer, O. *Chem. Ber.* **1977**, *110*, 3438. (m) Fahey, D. R.; Mahan, J. E. U.S. Patent 4,115,470, 1978. (n) Schmid, G. *J. Chem. Soc., Dalton Trans.* **1978**, 1387. (o) Langenbach, H.-J.; Vahrenkamp, H. *Chem. Ber.* **1979**, *112*, 3390. (p) Beysel, G.; Grobe, J.; Mohr, W. *J. Organomet. Chem.* **1979**, *170*, 319. (q) Petersen, J. L.; Stewart, R. P. *Inorg. Chem.* **1980**, *19*, 186. (r) Burckett-St. Laurent, J. C. T. R.; Haines, R. J.; Nolte, C. R.; Steen, N. D. C. T. *Ibid.* **1980**, *19*, 577. (s) Braunstein, P.; Matt, D.; Bars, O.; Louer, M.; Grandjean, D.; Fischer, J.; Mitschler, A. *J. Organomet. Chem.* **1981**, *213*, 79. (t) Natarajan, K.; Zsolnai, L.; Huttner, G. *J. Organomet. Chem.* **1981**, *220*, 265. (u) Young, D. A. *Inorg. Chem.* **1981**, *20*, 2049. (v) Collman, J. P.; Rothrock, R. K.; Finke, R. G.; Moore, E. J.; Rose-Munch, F. *Ibid.* **1982**, *21*, 146. (w) Regragui, R.; Dixneuf, P. H. *J. Organomet. Chem.* **1982**, *239*, C12. (x) Carty, A. J. *Adv. Chem. Ser.* **1982**, *No. 196*, 163. (y) Weber, D.; Fluck, E.; von Schnering, H.-G.; Peters, K. *Z. Naturforsch.* **1982**, *37b*, 594. (z) Jones, R. A.; Stuart, A. L.; Atwood, J. L.; Hunter, W. E.; Rogers, R. D. *Organometallics* **1982**, *1*, 1721. (aa) Bellon, P. L.; Ceriotti, A.; Demartin, F.; Longoni, G.; Heaton, B. E. *J. Chem. Soc., Dalton Trans.* **1982**, 1671. (bb) Roberts, D. A.; Geoffroy, G. L. In *Comprehensive Organometallic Chemistry*; Wilkinson, G., Stone, F. G. A., Abel, E. W., Eds.; Pergamon Press: Oxford, 1982; Chapter 40. (cc) Schafer, H.; Zipfel, J.; Migula, B.; Binder, D. *Z. Anorg. Allg. Chem.* **1983**, *501*, 111. (dd) Finke, R. G.; Gaughan, G.; Pierpont, C.; Noordik, J. H. *Organometallics* **1983**, *2*, 846. (ee) Yu, Y.; Galluci, J.; Wojcicki, A. *J. Am. Chem. Soc.* **1983**, *105*, 4826. (ff) Lau, C. P.; Ren, C. Y.; Book, L.; Mak, T. C. W. *J. Organomet. Chem.* **1983**, *249*, 429. (gg) Adams, R. D.; Horvath, I. T.; Segmuller, B. E. *Ibid.* **1984**, *262*, 243. (hh) Kyba, E. P.; Mather, J. D.; Hassett, K. L.; McKennis, J. S.; Davis, R. E. *J. Am. Chem. Soc.* **1984**, *106*, 5371. (ii) Glaser, R.; Kountz, D. J.; Waid, R. D.; Gallucci, J. C.; Meek, D. W. *Ibid.* **1984**, *106*, 6324. (jj) Henrick, K.; Iggo, J. A.; Mays, M. J.; Raithby, P. R. *J. Chem. Soc., Dalton Trans.* **1984**, 209. (kk) Bushnell, G. W.; Stobart, S. R.; Vefghi, R.; Zaworotko, M. J. *J. Chem. Soc., Chem. Commun.* **1984**, 282. (ll) Powell, J.; Gregg, M. R.; Sawyer, J. F. *Ibid.* **1984**, 1149. (mm) King, R. B.; Fu, W.-K.; Holt, E. M. *Ibid.* **1984**, 1439. (nn) Eichbichler, J.; Peringer, P. *Chem. Ber.* **1984**, *117*, 1215. (oo) Gross, E.; Jorg, K.; Fiederling, K.; Gottlein, A.; Malisch, W.; Boese, R. *Angew. Chem., Intl. Ed. Engl.* **1984**, *23*, 738. (pp) Werner, H.; Hofmann, W.; Zolk, R.; Dahl, L. F.; Kocal, J.; Kuhn, A. *J. Organomet. Chem.* **1985**, *239*, 173. (qq) Sabo, S.; Chaudret, B.; Gervais, D. *Ibid.* **1985**, *292*, 411. (rr) Lindner, E.; Goth, D. *Chem. Ber.* **1986**, *119*, 3859. (ss) Roddick, D. M.; Santarsiero, B. D.; Bercaw, J. E. *J. Am. Chem. Soc.* **1985**, *107*, 4670. (tt) Siedle, A. R.; Newmark, R. A.; Gleason, W. B. *Ibid.* **1986**, *108*, 767. (uu) Bruce, M. I.; Snow, M. R.; Tiekink, E. R. T.; Williams, M. L. *J. Chem. Soc., Chem. Commun.* **1986**, 701. (vv) Pritchard, R. G.; Dyson, D. B.; Parish, R. V.; McAuliffe, C. A.; Beagley, B. *Ibid.* **1987**, 371. (ww) Caminade, A.-M.; Majoral, J.-P.; Sanchez, M.; Mathieu, R.; Attali, S.; Grand, A. *Organometallics*, **1987**, *6*, 1459. (xx) Seyferth, D.; Wood, T. G. *Ibid.* **1987**, *6*, 2563. (yy) Buhro, W. E.; Chisholm, M. H.; Folting, K.; Eichorn, B. W.; Huffman, J. C. *J. Chem. Soc., Chem. Commun.* **1987**, 845. (zz) Baker, R. T.; Calabrese, J. C.; Glassman, T. E. *Organometallics* **1988**, *7*, 1889.

(2) Jones, R. A.; Lasch, J. G.; Norman, N. C.; Whittlesey, B. R.; Wright, T. C. *J. Am. Chem. Soc.* **1983**, *105*, 6184.

(3) Carty, A. J.; Hartstock, F.; Taylor, N. J. *Inorg. Chem.* **1982**, *21*, 1349.

(4) $Cp_2M(PR_2)_x$: (a) (M = Ti, Zr, Hf) Baker, R. T.; Whitney, J. F.; Wreford, S. S. *Organometallics* **1983**, *2*, 1049; *Inorg. Chem.*, submitted for publication. (b) (M = Sc, Y, Lu) Baker, R. T.; Calabrese, J. C.; Glassman, T. E. Manuscript in preparation.

(5) $Cp^*M(PR_2)_x$: (a) (M = Ti, Zr, Hf) Baker, R. T.; Krusic, P. J; Calabrese, J. C.; Ortiz, J. V. Manuscript in preparation. (b) (M = Ta, Mo, W) Baker, R. T.; Calabrese, J. C.; Harlow, R. L.; Williams, I. D. Manuscript in preparation.

(6) $M_x(PR_2)_y$: Baker, R. T.; Calabrese, J. C.; Krusic, P. J.; Tulip, T. H.; Wreford, S. S. *J. Am. Chem. Soc.* **1983**, *105*, 6763.

(7) Baker, R. T.; Tulip, T. H.; Wreford, S. S. *Inorg. Chem.* **1985**, *24*, 1379.

(8) Baker, R. T.; Fultz, W. C.; Tulip, T. H. 190th National ACS Meeting, Chicago, IL 1985; Abs INOR 269.

(9) Williams, I. D.; Marder, T. B. 3rd North American Chemical Congress, Toronto, Ontario 1988; Abs INOR 85.

(10) The syntheses of $Cp_2Zr(\mu\text{-}PPh_2)_2ML_n$ (M = Ni, Pd, Pt; L = PPh_3, RC≡CR) have been reported; however, no structural results were presented: (a) Stephan, D. L.; Gelmini, L. *Inorg. Chem.* **1986**, *25*, 1222. (b) Stephan, D. L.; Gelmini, L. *Inorg. Chim. Acta* **1986**, *111*, L17.

(11) Coulson, D. R. *Inorg. Synth.* **1972**, *13*, 121.

(12) Tatsuno, Y.; Yoshida, T.; Otsuka, A. *Inorg. Synth.* **1979**, *19*, 220.

(13) Spencer, J. L. *Inorg. Synth.* **1979**, *19*, 213.

(14) Ugo, R.; Cariati, F.; La Monica, G. *Inorg. Synth.* **1968**, *11*, 105.

Table I. ^{1}H NMR Spectral Data[a]

complex	no.	chemical shift, δ: Cp[b]	R: CH_2	R: CH_3	L
$Cp_2Hf(\mu\text{-}PEt_2)_2Ni(COD)$[d]	**1a**	4.93 (tr, 1.1)	1.93, 1.77 (m)	1.40 (d tr, 12.0, 7.5)	3.48 (br s, —CH=), 2.71, 2.55 (m, $-CH_2-$)
$Cp_2Hf(\mu\text{-}PEt_2)_2Ni(COD)$[d]	**1b**	4.88 (tr, 1.1)	1.94, 1.72 (m)	1.37 (d tr, 12.3, 7.4)	3.46 (br s, —CH=), 2.70, 2.55 (m, $-CH_2-$)
$Cp_2Hf(\mu\text{-}PEt_2)_2Ni(PMe_3)_2$[d]	**1c**	5.13	1.88, 1.78 (ov m)	1.42 (d tr, 12.5, 7.0)	1.04 (d, $^2J_{HP}$ = 1.5 Hz)
$Cp_2Hf(\mu\text{-}PEt_2)_2Ni[P(OMe)_3]_2$	**1d**	5.22	2.00, 1.79 (m)	1.38 (d tr, 13.0, 7.0)	3.54 (tr, J = 4.5 Hz)
$Cp_2Hf(\mu\text{-}PEt_2)_2Ni(DMPE)$[c]	**1f**	5.12	1.78 (ov m)	1.39 (d tr, 12.5, 7.0)	1.52 (m, 4 H, CH_2), 0.97 (d, $^2H_{HP}$ = 2 Hz, 12 H, CH_3)

complex	no.	Cp[b]	ortho	meta	para	L
$Cp_2Hf(\mu\text{-}PPh_2)_2Pd(DMPE)$	**1g**	5.16	7.63	7.18	7.07	1.61 (m, 4 H, CH_2), 0.94 (s, 12 H, CH_3)
$Cp_2Zr(\mu\text{-}PPh_2)_2Pt(DMPE)$	**1h**	5.15	7.61	7.17	7.08	1.54 (m, 4 H, CH_2), 0.95 (s, 12 H, CH_3)
$Cp_2Zr(\mu\text{-}PPh_2)_2Pd[P(OMe)_3]_2$	**1i**	5.08	7.72	7.25	7.14	3.49 (d, $^3J_{HP}$ = 11 Hz, 18 H)
$[Cp_2Hf(\mu\text{-}PP)]_2Ni$	**2d**	5.35	7.58 (m, 8 H, ortho), 7.09 (ov m, 12 H, meta and para),			2.56, 2.22, 1.67 (m, 4 H, $-CH_2$)

$[Cp_2M(\mu\text{-}PEt_2)_2]_2M'$ M	M′	no.	chemical shift, δ: Cp[b]	CH_2	CH_3	L
Zr	Ni[d]	**2a**	5.26	1.81, 1.58 (m)	1.12 (d tr, 6.9, 11.8)	
Hf	Ni[d]	**2b**	5.22	1.81, 1.64 (m)	1.13 (d tr, 7.5, 12.0)	
Zr/Hf	Ni[d]	**2c**	5.25, 5.23	1.83, 1.80, 1.63, 1.59 (ov m)	1.13, 1.11 (ov m)	
Zr	Pd[d]	**2e**	5.26	1.87, 1.64 (m)	1.15 (d tr, 6.8, 11.7)	
Hf	Pd[d]	**2f**	5.21	1.85, 1.68 (m)	1.16 (m)	
Zr	Pt[d]	**2g**	5.22	1.81, 1.50 (m)	1.12 (d tr, 6.5, 12.5)	
Hf	Pt[d]	**2h**	5.18	1.80, 1.54 (m)	1.13 (d tr, 6.9, 12.3)	

$Cp_2M(\mu\text{-}PR_2)_2M'(PR'_3)$ M	R	M′	R′	no.	chemical shift, δ: Cp[b]	R: CH_2	ortho	meta	para
Zr	Cy	Pd	Ph[d]	**3g**	5.57	2.2–1.1 (ov m)	7.73	7.15	7.05
Hf	Cy	Pd	Ph[d]	**3h**	5.51 (1.0)	2.2–1.0 (ov m)	7.74	7.15	7.05
Zr	Cy	Pt	Ph[d]	**3i**	5.57	2.2–1.1 (ov m)	7.71	7.15	7.04
Hf	Cy	Pt	Ph[d]	**3j**	5.52	2.3–1.1 (ov m)	7.72	7.15	7.05
Zr	Ph	Pd	Ph	**3k**	5.12	7.50 (ov m, 14 H, ortho), 7.23 (m, 4 H, para of PPh_2), 7.10 (ov m, 17 H, meta and para)			
Hf	Ph	Pd	Ph	**3l**	5.11 (1.5)	7.54 (m, 6 H, ortho of PPh_3), 7.48 (m, 8 H, ortho of PPh_2), 7.22 (m, 4 H, para of PPh_2), 7.06 (ov m, 17 H, meta and para)			
Zr	Ph	Pt	Ph	**3m**	5.03	7.45 (ov m, 14 H, ortho), 7.17 (m, 4 H, para of PPh_2), 7.04 (ov m, 17 H, meta and para)			
Hf	Ph	Pt	Ph	**3n**	5.05 (1.5)	7.54 (m, 6 H, ortho of PPh_3), 7.51 (m, 8 H, ortho of PPh_2), 7.20 (m, 4 H, para of PPh_2), 7.07 (ov m, 17 H, meta and para)			

M	R	M′	R′	no.	chemical shift, δ: Cp[b]	ortho	meta	para	L
Zr	Ph	Pd	Me	**3o**	5.05 (1.0)	7.67	7.22	7.12	1.55 (d, $^2J_{HP}$ = 5 Hz)
Zr	Ph	Pd	Cy	**3p**	5.04 (1.0)	7.59	7.24	7.12	2.15–0.8 (ov m)
Hf	Ph	Pt	Me	**3s**	4.95 (1.5)	7.76	7.24	7.12	1.78 (d, $^2J_{HP}$ = 4.5 Hz)
Hf	Ph	Pt	Cy	**3t**	4.93 (1.5)	7.67	7.25	7.12	2.2–0.8 (ov m)
Hf	Ph	Pt	OMe	**3u**	5.00 (1.5)	7.79	7.26	7.14	3.51 (d, $^3J_{HP}$ = 13 Hz)
Zr	Ph	Pt	O-*o*-tol	**3v**	5.02	7.60	7.14 (ov m)		7.36 (d, $^2J_{HH}$ = 8 Hz, 3 H), 6.98 (d, 7.5 Hz, 3 H), 6.74 (tr, 7.5 Hz, 3 H), 6.59 (dd, 8.0, 7.5 Hz, 3 H), 2.04 (s, 9 H, CH_3)

[a] Recorded at 25 °C in THF-d_8. [b] Singlet or triplet with $^2J_{HP}$ in hertz in parentheses. [c] $^3J_{HP}$, $^3J_{HH}$ in hertz in parentheses. [d] Recorded in C_6D_6.

turned red-purple. After stirring for 18 h, the solvent was removed in vacuo, and the resulting red-purple solid was washed with 15 mL of hexane and vacuum-dried, yielding 258 mg of **2d** (85%).

$Cp_2Hf(\mu\text{-}PEt_2)_2Ni(PMe_3)_2$ (1c). A solution of 60 mg (0.8 mmol) PMe_3 in 2 mL of THF was added dropwise to a solution of 260 mg (0.4 mmol) of $Cp_2Hf(\mu\text{-}PEt_2)_2Ni(1,5\text{-}COD)$ in 5 mL of THF. After stirring for 18 h, the solvent was removed in vacuo, and the resulting yellow–orange solid was stirred with 3 mL of hexane, filtered, and dried in vacuo, yielding 67 mg. Cooling the resulting filtrate at −30 °C for 12 h yielded a second crop of 58 mg. The total yield of **1c** was 125 mg (45%). The $P(OMe)_3$ analogue **1d**, was prepared similarly by using 110 mg (0.9 mmol) of $P(OMe)_3$ and 260 mg (0.4 mmol) of $Cp_2Hf(\mu\text{-}PEt_2)_2Ni(1,5\text{-}COD)$ to give 193 mg of a yellow solid (61%). The DMPE analogue **1f**, was prepared similarly by using 60 mg (0.4 mmol) of DMPE and 260 mg (0.4 mmol) of $Cp_2Hf(\mu\text{-}PEt_2)_2Ni(1,5\text{-}COD)$ to yield 148 mg of orange crystals (53%).

Generation of $Cp_2Hf(\mu\text{-}PEt_2)_2Ni[P(O\text{-}o\text{-}tol)_3]_n$ (n = 1 (3a), 2 (1e)). To a solution of 26 mg (0.04 mmol) of $Cp_2Hf(\mu\text{-}PEt_2)_2Ni(1,5\text{-}COD)$ in 1 mL of THF-d_8 was added 14 mg (0.04 mmol) of $P(O\text{-}o\text{-}tol)_3$. The solution turned dark red. The ^{31}P NMR spectrum was recorded, another 14 mg $P(O\text{-}o\text{-}tol)_3$ was added, and the spectrum was recorded again. Attempted isolation of the mono- and bis(phosphite) adducts was unsuccessful due to ligand redistribution (see text). The PCy_3 1:1 adduct, **3b**, was generated similarly from 26 mg (0.04 mmol) of $Cp_2Hf(\mu\text{-}PEt_2)_2Ni(1,5\text{-}COD)$ and 11 mg (0.04 mmol) PCy_3 in 1 mL of THF-d_8 and characterized by ^{31}P NMR spectroscopy.

$[Cp_2Zr(\mu\text{-}PEt_2)_2]_2Pd$ (2e). A solution of 400 mg (1.0 mmol) of $Cp_2Zr(PEt_2)_2$ in 5 mL of THF was added dropwise to 578 mg

Table II. $^{31}P\{^1H\}$ NMR Spectral Data[a]

$Cp_2M(\mu\text{-}PR_2)_2M'L_2$					chemical shift,[b] ppm	
M	R	M′	L_2	no.	PR_2	L
Zr	Et	Ni	1,5-COD	**1a**	148.6	
Hf	Et	Ni	1,5-COD	**1b**	136.5	
Hf	Et	Ni	$(PMe_3)_2$	**1c**	131.3 (tr, 16)	−15.8 (tr)
Hf	Et	Ni	$\{P(OMe)_3\}_2$	**1d**	134.0 (tr, 29)	154.3 (tr)
Hf	Et	Ni	$\{P(O\text{-}o\text{-}tol)_3\}_2$[c]	**1e**	126.4 (tr, 26)	124.2 (tr)
Hf	Et	Ni	DMPE[d]	**1f**	141.3 (tr, 15)	15.3 (tr)
Hf	Ph	Pd	DMPE	**1g**	148.0 (tr 20)	−11.6 (tr)
Zr	Ph	Pt	DMPE	**1h**	142.2 (tr, 2, 2571)	−17.6 (tr, 2879)
Zr	Ph	Pd	$\{P(OMe)_3\}_2$[e]	**1i**	157.1 (tr, 34)	151.8 (tr)

$[Cp_2M(\mu\text{-}PEt_2)_2]_2M'$			chemical shift,[b] ppm
M	M′	no.	PR_2
Zr	Ni	**2a**	134.1
Hf	Ni	**2b**	125.6
Zr/Hf	Ni	**2c**	135.1, 124.2 (tr, 20)
Zr	Pd	**2e**	138.4
Hf	Pd	**2f**	124.9
Zr	Pt	**2g**	106.6 (s, 2006)
Hf	Pt	**2h**	94.4 (s, 1984)
Zr/Hf	Pd	**2i**	139.9, 123.2 (tr, 20)
Zr/Hf	Pt	**2j**	108.1 (tr, 25, 2026), 92.6 (tr, 1981)

$[Cp_2M(\mu\text{-}PP)]_2M'$			chemical shift,[b] ppm
M	M′	no.	PR_2
Hf	Ni	**2d**	118.3 (s)

$Cp_2M(\mu\text{-}PR_2)_2M'(PR'_3)$					chemical shift,[b] ppm	
M	R	M′	R′	no.	PR_2	L
Hf	Et	Ni	O-*o*-tol[c]	**3a**	88.5 (d, 12)	145.4 (tr)
Hf	Et	Ni	Cy	**3b**	85.2 (s)	46.0 (s)
Zr	Et	Pd	Ph	**3c**	102.7	29.5
Hf	Et	Pd	Ph	**3d**	85.7	29.2
Zr	Et	Pt	Ph	**3e**	105.5 (s, 2334)	46.3 (s, 3950)
Hf	Et	Pt	Ph	**3f**	86.6 (d, 6, 2262)	47.7 (tr, 3886)
Zr	Cy	Pd	Ph	**3g**	147.5 (d, 22)	29.3 (tr)
Hf	Cy	Pd	Ph	**3h**	127.4 (d, 22)	30.4 (tr)
Zr	Cy	Pt	Ph	**3i**	136.5 (d, 10, 2263)	45.1 (tr, 3762)
Hf	Cy	Pt	Ph	**3j**	115.9 (d, 14, 2199)	47.4 (tr, 3699)
Zr	Ph	Pd	Ph	**3k**	122.9 (d, 18)	29.1 (tr)
Hf	Ph	Pd	Ph[d]	**3l**	109.3 (d, 19)	29.9 (tr)
Zr	Ph	Pt	Ph	**3m**	122.7 (s, 2677)	50.8 (s, 3987)
Hf	Ph	Pt	Ph[d]	**3n**	106.7 (d, 5, 2616)	52.6 (tr, 3943)
Zr	Ph	Pd	Me[d]	**3o**	125.2 (s)	−30.2 (s)
Zr	Ph	Pd	Cy[d]	**3p**	122.0 (d, 18)	46.6 (tr)
Zr	Ph	Pd	OMe[e]	**3q**	127.9 (br s)	171.1 (br s)
Hf	Ph	Pd	O-*o*-tol[d]	**3r**	110.7 (d, 32)	145.2 (tr)
Hf	Ph	Pt	Me[d]	**3s**	112.0 (s, 2607)	−4.9 (s, 3881)
Hf	Ph	Pt	Cy[d]	**3t**	110.8 (s, 2733)	67.3 (s, 3899)
Hf	Ph	Pt	OMe[d]	**3u**	112.3 (s, 2522)	194.7 (s, 6528)
Zr	Ph	Pt	O-*o*-tol[d]	**3v**	124.6 (d, 4, 2601)	164.8 (tr, 6859)

[a] Recorded in C_6D_6 at 25 °C with proton decoupling. Abbreviations: PP = $PhP(CH_2)_3PPh$, Cy = cyclohexyl, tol = tolyl, DMPE = $(Me_2PCH_2)_2$, COD = cyclooctadiene. [b] Multiplicity, $^2J_{PP}$, J_{PPt} in hertz in parentheses. [c] Recorded at −30 °C in THF-d_8. [d] Recorded in THF-d_8. [e] Recorded at −98 °C in THF-d_8.

(0.5 mmol) of $Pd(PPh_3)_4$ suspended in 5 mL of THF. The solution turned red. Upon standing for 3 days, the red crystals were filtered off, washed with 5 mL of cold pentane, and dried in vacuo, yielding 194 mg (41% based on **2e**·$^1/_2$THF). The Hf analogue, **2f**, was prepared similarly by using 487 mg (1.0 mmol) of $Cp_2Hf(PEt_2)_2$, yielding 175 mg of red-orange crystals (31%). The yields of **2e,f** are essentially quantitative using the less readily available starting material CpPd(η-2-Me-allyl).

$[Cp_2Zr(\mu\text{-}PEt_2)_2]_2Pt$ (2g). A solution of 400 mg (1.0 mmol) of $Cp_2Zr(PEt_2)_2$ in 5 mL of THF was added dropwise to 491 mg (0.5 mmol) of $Pt(PPh_3)_3$ suspended in 5 mL of THF. The solution turned red. Upon standing for 3 days, the red-orange crystals were filtered off, washed with 5 mL of cold pentane, and dried in vacuo, yielding 249 mg (47%). The Hf analogue, **2h**, was prepared similarly by using 487 mg (1.0 mmol) of $Cp_2Hf(PEt_2)_2$, yielding 330 mg of orange crystals (53%). The yields of **2g,h** are essentially quantitative using the less readily available starting material, $Pt(1,5\text{-}COD)_2$.

Generation of $Cp_2Zr(\mu\text{-}PEt_2)_2M(\mu\text{-}PEt_2)_2HfCp_2$ (M = Pd (2i), Pt (2j)). A solution of 60 mg (0.15 mmol) of $Cp_2Zr(PEt_2)_2$ in 3 mL of THF was added dropwise to 174 mg (0.15 mmol) of $Pd(PPh_3)_4$ in 1 mL of THF. The solution turned red-orange. A solution of 73 mg (0.15 mmol) of $Cp_2Hf(PEt_2)_2$ in 3 mL of THF was then added. After stirring for 10 min, the solvent was removed in vacuo and the residue was dissolved in 2.5 mL of THF-d_8. The heterotrimetallic product, **2i**, was characterized spectroscopically by ^{31}P NMR, and no attempt was made to separate **2i** from accompanying **2e,f** and PPh_3. The Pt analogue, **2j**, was generated and characterized similarly by using 147 mg (0.15 mmol) of $Pt(PPh_3)_3$.

Generation of $Cp_2Zr(\mu\text{-}PEt_2)_2Pd(PPh_3)$ (3c). A solution of 400 mg (1.0 mmol) of $Cp_2Zr(PEt_2)_2$ in 250 mL of THF was added dropwise over 5 h to a solution of 1.156 g (1.0 mmol) of $Pd(PPh_3)_4$ in 100 mL of THF cooled to 0 °C. After warming slowly to ambient temperature and stirring for a total of 20 h, the solvent was removed in vacuo. The orange residue was extracted with 2 × 50 mL of cold (−30 °C) pentane. Cooling the extracts at −30 °C for 48 h yielded 654 mg of an orange solid. ^{31}P NMR of this solid indicated it to be initially >80% **3c**, contaminated with PPh_3 and **2e**; upon standing, **3c** slowly converted to **2e** and $Pd(PPh_3)_n$.

Table III. Summary of X-ray Diffraction Data

	$Cp_2Zr(\mu\text{-}PEt_2)_2Ni(\mu\text{-}PEt_2)_2HfCp_2 \cdot {}^1/_2THF$ (**2c**)	$Cp_2Hf(\mu\text{-}PPh_2)_2Pd(PPh_3)$ (**3l**)	$Cp_2Hf(\mu\text{-}PPh_2)_2Pd(DMPE)$ (**1g**)
formula	$C_{38}H_{64}HfNiO_{0.5}P_4Zr$	$C_{52}H_{45}HfP_3Pd$	$C_{40}H_{46}HfP_4Pd$
fw	981.25	1047.74	935.59
a, Å	34.823 (4)	27.701 (8)	25.361 (12)
b, Å	10.991 (2)	10.654 (5)	19.584 (5)
c, Å	21.606 (3)	30.330 (11)	18.814 (13)
β, deg	105.65 (1)	103.16 (5)	126.14 (5)
V, Å^3	7964.27	8716	7546.8
Z	8	8	8
ρ_{calcd}, g cm^{-3}	1.6365	1.597	1.647
space group	$C2/c$ (No. 15)	$C2/c$ (No. 15)	$C2/c$ (No. 15)
cryst dimens, mm	0.26 × 0.15 × 0.34	0.22 × 0.25 × 0.42	0.30 × 0.24 × 0.40
temp, °C	−100	−100	−75
radiation	Mo Kα	Mo Kα	Mo Kα
μ, cm^{-1}	34.869	29.097	33.90
data coll method	ω–2θ	ω–2θ	ω–2θ
max 2θ, deg	52.0	55.0	55.0
scan speed, (deg/min)	4.0–10.0	4.0–15.0	1.70–6.70
scan width			1.20–1.50ω
total no. of obsvns	8611	11069	16090
no. of unique data ($I > 3\sigma(I)$)	6283	5372	5677
final no. of variables	411	515	415
final max shift/error			0.42
max residual density, e/Å^3	0.70	0.35	1.33
R^a	0.038	0.028	0.037
$R_w{}^b$	0.040	0.029	0.043

$^a \sum||F_o| - |F_c||/\sum|F_o|$. $^b [\sum w(|F_o| - |F_c|)^2/\sum wF_o^2]^{1/2}$.

Similar results were obtained for the Hf analogue, **3d**.

$Cp_2Zr(\mu\text{-}PCy_2)_2Pd(PPh_3)$ (3g). To a solution of 75 mg (0.33 mmol) of CpPd(η-2-Me-allyl) and 87 mg (0.33 mmol) PPh_3 in 10 mL of THF was added dropwise a solution of 205 mg (0.33 mmol) of $Cp_2Zr(PCy_2)_2$ in 5 mL of THF. The solution turned orange-brown. After 40 h, 10 mL of heptane was added, and the solution concentrated to 10 mL and filtered. The resulting yellow powder was washed with cold (−20 °C) pentane and dried in vacuo to yield 194 mg (60%). The Hf analogue, **3h**, was prepared similarly by using 75 mg of CpPd(η-2-Me-allyl), 87 mg PPh_3, and 233 mg (0.33 mmol) $Cp_2Hf(PCy_2)_2$ to yield 155 mg (44%).

$Cp_2Zr(\mu\text{-}PPh_2)_2Pd(PPh_3)$ (3k). To a solution of 75 mg (0.33 mmol) of CpPd(η-2-Me-allyl) and 87 mg (0.33 mmol) of PPh_3 in 10 mL of THF was added dropwise a solution of 196 mg (0.33 mmol) of $Cp_2Zr(PPh_2)_2$ in 5 mL of THF. The solution turned red-orange. After stirring for 20 h, the solvent was removed in vacuo, and the resulting orange solid was washed with 2 × 10 mL of pentane and dried in vacuo, yielding 250 mg (79%). The complex can be recrystallized from THF–hexane to give large red crystals. The Hf analogue, **3l**, was prepared similarly by using 75 mg of CpPd(η-2-Me-allyl), 87 mg of PPh_3, and 227 mg (0.33 mmol) of $Cp_2Hf(PPh_2)_2$, yielding 289 mg (84%).

$Cp_2Zr(\mu\text{-}PCy_2)_2Pt(PPh_3)$ (3i). To a solution of 135 mg (0.33 mmol) of Pt(1,5-COD)$_2$ and 87 mg (0.33 mmol) of PPh_3 in 5 mL of THF was added a solution of 205 mg (0.33 mmol) of $Cp_2Zr(PCy_2)_2$ in 10 mL of THF. The solution turned red-orange. After stirring for 40 h, the solvent was removed in vacuo, and 2 mL of hexane was added to the residue. The resulting orange solid was filtered off, washed with cold pentane, and dried in vacuo to yield 229 mg (65%). The Hf analogue, **3j**, was prepared similarly by using 135 mg of Pt(1,5-COD)$_2$, 87 mg of PPh_3 and 235 mg (0.33 mmol) of $Cp_2Hf(PCy_2)_2$ to yield 297 mg (78%).

$Cp_2Zr(\mu\text{-}PPh_2)_2Pt(PPh_3)$ (3m). To a solution of 135 mg (0.33 mmol) of Pt(1,5-COD)$_2$ and 87 mg (0.33 mmol) of PPh_3 in 5 mL of THF was added a solution of 198 mg (0.33 mmol) of $Cp_2Zr(PPh_2)_2$ in 10 mL of THF. The solution turned red-orange. After stirring for 18 h, the solvent was removed in vacuo, and the resulting orange solid was stirred with 3 mL of hexane for 1 h, filtered, washed with 10 mL of cold pentane, and dried in vacuo to yield 283 mg (82%). The complex can be recrystallized from THF–hexane to give large red crystals. The Hf analogue, **3n**, was prepared similarly by using 135 mg of Pt(1,5-COD)$_2$, 87 mg of PPh_3, and 227 mg (0.33 mmol) of $Cp_2Hf(PPh_2)_2$, yielding 249 mg of a yellow-orange solid (66%).

$Cp_2Zr(\mu\text{-}PPh_2)_2Pt(PMe_3)$ (3o). To a solution of 75 mg (0.33 mmol) of CpPd(η-2-Me-allyl) and 50 mg (0.66 mmol) of PMe_3 in 10 mL of THF was added a solution of 198 mg (0.33 mmol) of $Cp_2Zr(PPh_2)_2$ in 10 mL of THF. The solution turned red-orange. After stirring for 18 h, 10 mL of heptane was added, and the solution was concentrated in vacuo to 10 mL. The resulting orange solid was filtered off, washed with 5 mL of cold pentane, and dried in vacuo to yield 198 mg (77%). The PCy_3 analogue, **3p**, was prepared similarly by using 75 mg of CpPd(η-2-Me-allyl), 93 mg (0.33 mmol) of PCy_3, and 198 mg of $Cp_2Zr(PPh_2)_2$ to give 264 mg of an orange solid (82%). The Hf–Pt–PMe_3 analogue, **3s**, was prepared similarly by using 135 mg of Pt(1,5-COD)$_2$, 50 mg of PMe_3, and 227 mg (0.33 mmol) of $Cp_2Hf(PPh_2)_2$ to yield 217 mg of an orange solid (69%). The Hf–Pt–PCy_3 analogue, **3t**, was prepared similarly by using 135 mg of Pt(1,5-COD)$_2$, 93 mg of PCy_3, and 227 mg of $Cp_2Hf(PPh_2)_2$ to give 256 mg of an orange-brown solid (67%). The Zr–Pt–P(O-*o*-tol)$_3$ analogue, **3v**, was prepared similarly by using 41 mg (0.1 mmol) of Pt(1,5-COD)$_2$, 36 mg (0.1 mmol) of P(O-*o*-tol)$_3$, and 59 mg (0.1 mmol) of $Cp_2Zr(PPh_2)_2$ to give 84 mg of an orange solid (74%).

$Cp_2Zr(\mu\text{-}PPh_2)_2Pd[P(OMe)_3]_n$ (n = 1 (3q), 2 (1i)). To a solution of 75 mg (0.33 mmol) of CpPd(η-2-Me-allyl) and 83 mg (0.66 mmol) of $P(OMe)_3$ in 5 mL of THF was added a solution of 198 mg (0.33 mmol) of $Cp_2Zr(PPh_2)_2$ in 10 mL of THF dropwise. The solution turned yellow. After stirring for 18 h, the solvent was removed in vacuo, and the residue was stirred with 5 mL of hexane, filtered, and dried in vacuo to yield 102 mg of a yellow solid. Spectroscopic characterization of the solid showed it to be a mixture of **3q** and **1i**.

$Cp_2Hf(PPh_2)_2Pd(DMPE)$ (1g). A solution of 31 mg (0.21 mmol) of DMPE in 2 mL of THF was added dropwise to a solution of 209 mg (0.2 mmol) of $Cp_2Hf(\mu\text{-}PPh_2)_2Pd(PPh_3)$ in 10 mL of THF. The solution turned red-orange. After stirring for 18 h, the solvent was removed in vacuo, and the residue stirred with 6 mL of hexane, filtered, and dried in vacuo to yield 132 mg of red-orange crystals (71%). The complex can be recrystallized from 1:5 THF–hexane. The Zr–Pt analogue, **1h**, was prepared similarly from 62 mg (0.41 mmol) of DMPE and 420 mg (0.4 mmol) of $Cp_2Zr(\mu\text{-}PPh_2)_2Pt(PPh_3)$ to give 303 mg of red crystals (81%).

Molecular Structure Determination. Crystals suitable for X-ray diffraction studies were obtained as described above. A summary of the crystallographic data is presented in Table III. All data sets were collected at low temperatures on automated diffractometers using graphite-monochromated Mo radiation. The data were reduced in the usual fashion for Lorentz polarization

Table IV. Selected Bond Distances (Å) and Angles (deg) for $Cp_2Zr(\mu\text{-}PEt_2)_2Ni(\mu\text{-}PEt_2)_2HfCp_2$ (2c)

M*(2)-Ni(1)	3.0186 (8)	M*(1)-C(74)	2.500 (6)
M*(2)-P(3)	2.605 (1)	M*(1)-C(75)	2.525 (6)
M*(2)-P(4)	2.600 (1)	M*(1)-C(81)	2.504 (6)
M*(2)-C(51)	2.508 (6)	M*(1)-C(82)	2.495 (6)
M*(2)-C(52)	2.523 (6)	M*(1)-C(83)	2.524 (6)
M*(2)-C(53)	2.511 (6)	M*(1)-C(84)	2.532 (6)
M*(2)-C(54)	2.532 (6)	M*(1)-C(85)	2.522 (6)
M*(2)-C(55)	2.521 (6)	Ni(1)-P(1)	2.234 (2)
M*(2)-C(61)	2.526 (6)	Ni(1)-P(2)	2.234 (2)
M*(2)-C(62)	2.517 (6)	Ni(1)-P(3)	2.244 (1)
M*(2)-C(63)	2.513 (6)	Ni(1)-P(4)	2.237 (1)
M*(2)-C(64)	2.517 (6)	P(1)-C(11)	1.857 (6)
M*(2)-C(65)	2.511 (6)	P(1)-C(15)	1.878 (6)
M*(1)-Ni(1)	3.0354 (9)	P(2)-C(21)	1.864 (5)
M*(1)-P(1)	2.595 (2)	P(2)-C(25)	1.866 (6)
M*(1)-P(2)	2.607 (1)	P(3)-C(31)	1.876 (6)
M*(1)-C(71)	2.530 (6)	P(3)-C(35)	1.867 (6)
M*(1)-C(72)	2.520 (6)	P(4)-C(41)	1.863 (6)
M*(1)-C(73)	2.501 (6)	P(4)-C(45)	1.860 (6)

P(1)-M*(1)-P(2)	91.80 (5)	M*(2)-P(3)-Ni(1)	76.60 (4)
M*(1)-Ni(1)-P(1)	56.58 (4)	M*(2)-P(4)-Ni(1)	76.82 (4)
M*(1)-Ni(1)-P(2)	56.88 (4)	M*(2)-P(3)-C(31)	116.9 (2)
M*(1)-Ni(1)-P(3)	122.15 (4)	M*(2)-P(3)-C(35)	120.8 (2)
M*(1)-Ni(1)-P(4)	123.77 (5)	M*(2)-P(4)-C(41)	120.9 (2)
Ni(1)-M*(1)-P(1)	45.92 (3)	M*(2)-P(4)-C(45)	118.3 (2)
Ni(1)-M*(1)-P(2)	45.88 (3)	P(1)-Ni(1)-P(2)	113.46 (6)
M*(1)-P(1)-Ni(1)	77.50 (5)	P(1)-Ni(1)-P(3)	107.20 (6)
M*(1)-P(2)-Ni(1)	77.24 (5)	P(1)-Ni(1)-P(4)	107.47 (6)
M*(1)-P(1)-C(11)	119.6 (2)	P(2)-Ni(1)-P(3)	107.35 (6)
M*(1)-P(1)-C(15)	120.4 (2)	P(2)-Ni(1)-P(4)	107.45 (6)
M*(1)-P(2)-C(21)	117.9 (2)	P(3)-Ni(1)-P(4)	114.08 (6)
M*(1)-P(2)-C(25)	121.2 (2)	Ni(1)-P(1)-C(11)	121.0 (2)
P(3)-M*(2)-P(4)	92.50 (4)	Ni(1)-P(1)-C(15)	123.5 (2)
M*(2)-Ni(1)-M*(1)	178.8 (2)	Ni(1)-P(2)-C(21)	122.4 (2)
M*(2)-Ni(1)-P(1)	122.55 (5)	Ni(1)-P(2)-C(25)	123.1 (2)
M*(2)-Ni(1)-P(2)	123.99 (5)	Ni(1)-P(3)-C(31)	124.6 (2)
M*(2)-Ni(1)-P(3)	57.08 (4)	Ni(1)-P(3)-C(35)	123.6 (2)
M*(2)-Ni(1)-P(4)	57.01 (4)	Ni(1)-P(4)-C(41)	123.9 (2)
Ni(1)-M*(2)-P(3)	46.33 (3)	Ni(1)-P(4)-C(45)	122.4 (2)
Ni(1)-M*(2)-P(4)	46.18 (3)	C(11)-P(1)-C(15)	96.9 (3)
		C(21)-P(2)-C(25)	96.9 (3)
		C(31)-P(3)-C(35)	96.2 (3)
		C(41)-P(4)-C(45)	96.5 (3)

and in the case of **1g** for a 25% decay in intensity. In addition, the data for **3l** and **1g** were treated for absorption via the $\Delta|F_o - F_c|$ method.[15] The solution and refinement of the structures were performed on a VAX/IBM cluster system using a local program set. For **3l** and **1g** the heavy-atom positions were obtained via automated Patterson analysis and used to phase the reflections for the remaining light atoms via the usual combination of structure factor, Fourier synthesis, and full-matrix least-squares refinement. Although the β angle for **1g** is large, the refinement converged satisfactorily using the standard space group setting, with no unreasonable correlations. For **2c** the structure was solved by direct methods[16] and displayed a disorder of the Zr and Hf positions. These were included in the refinement model by using a 1:1 Zr/Hf averaged scattering curve. All refinements were performed by using full-matrix least-squares on F, with anisotropic thermal parameters for all non-hydrogen atoms, and included anomalous dispersion terms[17] for all metal and P atoms as well as idealized hydrogen coordinates as fixed atom contributors. Selected bond distances and angles are given in Tables IV–VI. Metrical details of the three structures are compared with closely related structures in Table VII. The final positional and thermal parameters for the non-hydrogen atoms (Tables XI, XV and XIX), general temperature factors (Tables XII, XVI, and XX), calculated hydrogen atom positions (Tables XIII, XVII, and XXI), and

(15) Walker, N.; Stuart, D. *Acta Crystallogr.* **1983**, *A39*, 158.
(16) Gilmore, C. J. MITHRIL, a computer program for the automatic solution of crystal structures from X-ray data, University of Glasgow, Scotland, 1983.
(17) *International Tables for X-ray Crystallography*; Kynoch Press: Birmingham, England, 1974; Vol. IV, (a) Table 2.2B, (b) Table 2.31.

Table V. Selected Bond Distances (Å) and Angles (deg) for $Cp_2Hf(\mu\text{-}PPh_2)_2Pd(PPh_3)$ (3l)

Hf(1)-Pd(1)	2.896 (1)	Hf(1)-C(10)	2.489 (6)
Hf(1)-P(1)	2.627 (2)	Pd(1)-P(1)	2.316 (2)
Hf(1)-P(2)	2.615 (2)	Pd(1)-P(2)	2.318 (2)
Hf(1)-C(1)	2.501 (5)	Pd(1)-P(3)	2.327 (2)
Hf(1)-C(2)	2.499 (6)	P(1)-C(11)	1.830 (5)
Hf(1)-C(3)	2.469 (5)	P(1)-C(21)	1.828 (5)
Hf(1)-C(4)	2.484 (6)	P(2)-C(31)	1.836 (5)
Hf(1)-C(5)	2.486 (6)	P(2)-C(41)	1.842 (5)
Hf(1)-C(6)	2.480 (5)	P(3)-C(51)	1.839 (5)
Hf(1)-C(7)	2.486 (5)	P(3)-C(61)	1.827 (5)
Hf(1)-C(8)	2.521 (5)	P(3)-C(71)	1.833 (5)
Hf(1)-C(9)	2.519 (5)		

Pd(1)-Hf(1)-P(1)	49.29 (4)	Pd(1)-Hf(1)-P(2)	49.42 (5)
P(1)-Hf(1)-P(2)	97.01 (5)	Pd(1)-P(1)-C(11)	125.1 (2)
Hf(1)-Pd(1)-P(1)	59.29 (5)	Pd(1)-P(1)-C(21)	113.0 (2)
Hf(1)-Pd(1)-P(2)	58.95 (5)	Pd(1)-P(2)-C(31)	111.8 (2)
Hf(1)-Pd(1)-P(3)	166.20 (5)	Pd(1)-P(2)-C(41)	132.1 (2)
Hf(1)-P(1)-Pd(1)	71.43 (5)	Pd(1)-P(3)-C(51)	119.0 (2)
Hf(1)-P(2)-Pd(1)	71.63 (4)	Pd(1)-P(3)-C(61)	116.3 (2)
Hf(1)-P(1)-C(11)	118.1 (2)	Pd(1)-P(3)-C(71)	111.4 (2)
Hf(1)-P(1)-C(21)	125.8 (2)	C(11)-P(1)-C(21)	102.8 (2)
Hf(1)-P(2)-C(31)	115.0 (2)	C(31)-P(2)-C(41)	99.5 (2)
Hf(1)-P(2)-C(41)	126.3 (2)	C(51)-P(3)-C(61)	102.5 (2)
P(1)-Pd(1)-P(2)	115.82 (5)	C(51)-P(3)-C(71)	102.7 (2)
P(1)-Pd(1)-P(3)	118.60 (6)	C(61)-P(3)-C(71)	102.7 (2)
P(2)-Pd(1)-P(3)	125.56 (6)		

Table VI. Selected Bond Distances (Å) and Angles (deg) for $Cp_2Hf(\mu\text{-}PPh_2)_2Pd(DMPE)$ (1g)

Hf(1)-Pd(1)	2.983 (1)	Pd(1)-P(1)	2.303 (2)
Hf(1)-P(1)	2.618 (2)	Pd(1)-P(2)	2.313 (2)
Hf(1)-P(2)	2.607 (3)	Pd(1)-P(3)	2.400 (2)
Hf(1)-C(90)	2.498 (6)	Pd(1)-P(4)	2.383 (2)
Hf(1)-C(91)	2.471 (6)	P(1)-C(11)	1.841 (6)
Hf(1)-C(92)	2.504 (6)	P(1)-C(21)	1.830 (6)
Hf(1)-C(93)	2.503 (6)	P(2)-C(31)	1.837 (6)
Hf(1)-C(94)	2.507 (6)	P(2)-C(41)	1.832 (6)
Hf(1)-C(95)	2.491 (7)	P(3)-C(51)	1.806 (8)
Hf(1)-C(96)	2.496 (6)	P(3)-C(61)	1.805 (8)
Hf(1)-C(97)	2.506 (6)	P(3)-C(72)	1.820 (8)
Hf(1)-C(98)	2.485 (7)	P(4)-C(01)	1.782 (10)
Hf(1)-C(99)	2.490 (7)	P(4)-C(71)	1.807 (8)
		P(4)-C(81)	1.799 (8)

P(1)-Hf(1)-P(2)	94.26 (8)	P(2)-Pd(1)-P(4)	119.05 (7)
Hf(1)-Pd(1)-P(1)	57.68 (6)	P(3)-Pd(1)-P(4)	85.47 (6)
Hf(1)-Pd(1)-P(2)	57.31 (7)	Pd(1)-Hf(1)-P(1)	48.02 (6)
Hf(1)-Pd(1)-P(3)	121.51 (4)	Pd(1)-Hf(1)-P(2)	48.33 (5)
Hf(1)-Pd(1)-P(4)	152.54 (5)	Pd(1)-P(3)-C(51)	123.7 (3)
Hf(1)-P(1)-Pd(1)	74.30 (7)	Pd(1)-P(3)-C(61)	126.9 (3)
Hf(1)-P(2)-Pd(1)	74.36 (7)	Pd(1)-P(3)-C(72)	103.9 (3)
Hf(1)-P(1)-C(11)	124.1 (2)	Pd(1)-P(4)-C(01)	127.3 (4)
Hf(1)-P(1)-C(21)	119.4 (2)	Pd(1)-P(4)-C(71)	105.4 (3)
Hf(1)-P(2)-C(31)	124.9 (2)	Pd(1)-P(4)-C(81)	120.1 (3)
Hf(1)-P(2)-C(41)	117.9 (2)	C(11)-P(1)-C(21)	98.1 (3)
Pd(1)-P(1)-C(11)	126.0 (2)	C(31)-P(2)-C(41)	101.0 (3)
Pd(1)-P(1)-C(21)	116.2 (2)	C(51)-P(2)-C(61)	96.8 (4)
Pd(1)-P(2)-C(31)	122.0 (2)	C(51)-P(3)-C(72)	100.8 (5)
Pd(1)-P(2)-C(41)	116.6 (2)	C(61)-P(3)-C(72)	99.7 (5)
P(1)-Pd(1)-P(2)	112.09 (8)	C(01)-P(4)-C(71)	99.5 (6)
P(1)-Pd(1)-P(3)	113.83 (6)	C(01)-P(4)-C(81)	100.0 (6)
P(1)-Pd(1)-P(4)	109.27 (8)	C(71)-P(4)-C(81)	99.5 (4)
P(2)-Pd(1)-P(3)	114.68 (6)		

structure factor listings (Tables XIV, XVIII, and XXII) are available as supplementary material.

Results and Discussion

Synthesis. $Cp_2M(PEt_2)_2$ (1 equiv, M = Zr, Hf) reacts with Ni(1,5-COD)$_2$ to give 1,5-COD and the 1:1 complexes, $Cp_2M(\mu\text{-}PEt_2)_2Ni$(1,5-COD), **1a,b**; using 2 equiv gives the 2:1 complexes, $[Cp_2M(\mu\text{-}PEt_2)_2]_2Ni$ (**2a,b**, Scheme I). Reaction of **1a** (M = Zr) with $Cp_2Hf(PEt_2)_2$ affords the heterotrimetallic $Cp_2Zr(\mu\text{-}PEt_2)_2Ni(\mu\text{-}PEt_2)_2HfCp_2$, **2c**.

Table VII. X-ray Structural Data for $Cp_2M(\mu\text{-}PR_2)_2M'L_n$[a]

M	R	$M'L_n$	M-P	P-M-P	M'-P	P-M'-P	M-M'	M-P-M'	ϕ[b]	ref
Hf	Et	$Ni(PEt_2)_2ZrCp_2$	2.605	91.80	2.234	113.46	3.019	76.60	1.03	this work
			2.600	92.50	2.234	114.08	3.035	76.82	1.10	
			2.595		2.244			77.50		
			2.607		2.237			77.24		
Hf	Et	$Mo(CO)_4$	2.592	95.30	2.538	98.21	3.400	83.01	7.7	7
			2.596		2.534					
Hf	Ph	$Pd(PPh_3)$	2.627	97.01	2.316	115.82	2.896	71.43	24.49	this work
			2.615		2.318			71.63		
Hf	Ph	$RhH(CO)(PPh_3)$	2.640	96.4	2.339	117.4	2.964	73.2	9.73	19
			2.672		2.325			72.4		
Hf	Ph	Pd(DMPE)	2.618	94.26	2.303	112.09	2.983	74.30	27.25	this work
			2.607		2.313			74.36		
Zr	Ph	$Rh(\eta^5\text{-indenyl})$	2.590	91.95	2.264	110.66	3.088	78.70	NO	18
Zr	Ph	$W(CO)_4$	2.619	98.30	2.537	103.27	3.289	79.25	1.6	32
			2.631		2.529			79.16		
Zr	Ph	$Mo(CO)_4$	2.631	98.5	2.547	103.1	3.299	79.1	NO	32a
			2.630		2.543			79.2		

[a] Distances are in angstroms and angles in degrees. [b] The dihedral angle between MP_2 and $M'P_2$ planes. NO = not obtained.

Scheme I[a]

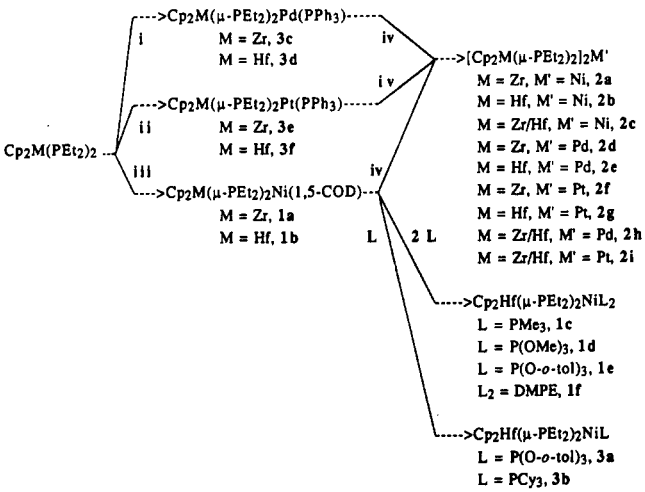

[a] (i) $Pd(PPh_3)_4$; (ii) $Pt(PPh_3)_3$; (iii) $Ni(1,5\text{-}COD)_2$; (iv) $Cp_2M(PEt_2)_2$; COD = cyclooctadiene, DMPE = $(Me_2PCH_2)_2$, Cy = cyclohexyl.

Whereas the bulkier ligands $Cp_2M(PR_2)_2$ (R = Cy, Ph) gave a mixture of incompletely characterized products, the cyclic bis(phosphine) $Cp_2Hf[PhP(CH_2)_3PPh]$ reacts with $Ni(1,5\text{-}COD)_2$ to yield the 2:1 complex, $\{Cp_2Hf[\mu\text{-}PhP(CH_2)_3PPh]\}_2Ni$, **2d**, regardless of the stoichiometry used.

Complex **1b** (M = Hf) also reacts with a variety of phosphine and phosphite ligands to yield both mono- and bis(ligand)-substituted products, $Cp_2Hf(\mu\text{-}PEt_2)_2NiL_n$ (n = 2; L = PMe_3 (**1c**), $P(OMe)_3$ (**1d**), $P(O\text{-}o\text{-}tol)_3$ (**1e**); n = 1; L = DMPE (**1f**), $P(O\text{-}o\text{-}tol)_3$ (**3a**), PCy_3 (**3b**)). While complexes **1c,d,f** were isolated and completely characterized, the mono(ligand) complexes were less stable and tended to undergo ligand redistribution to form **2b**.

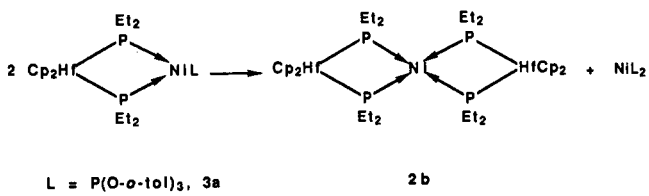

Reaction of 2 equiv of $Cp_2M(PEt_2)_2$ with $Pd(PPh_3)_4$ or $Pt(PPh_3)_3$ gives the 2:1 complexes **2e–h**, which crystallize out of the concentrated THF reaction solutions, allowing for their separation from excess PPh_3. With 1 equiv of $Cp_2M(PEt_2)_2$, a mixture of the 2:1 and the 1:1 mono-

Scheme II[a]

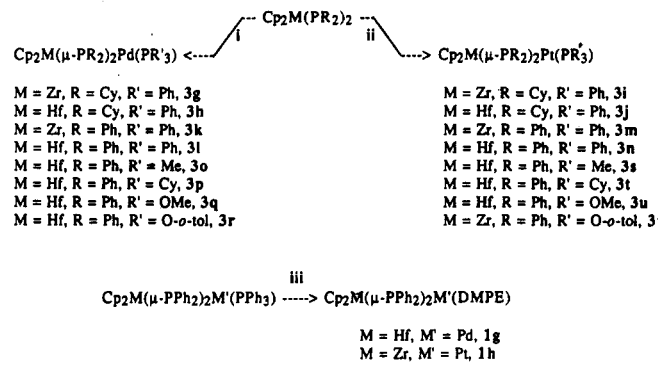

[a] (i) $CpPd(\eta\text{-}2\text{-}Me\text{-}allyl)/PR'_3$; (ii) $Pt(1,5\text{-}COD)_2/PR'_3$; (iii) DMPE. COD = cyclooctadiene, Cy = cyclohexyl, DMPE = $(Me_2PCH_2)_2$.

phosphine complexes, $Cp_2M(\mu\text{-}PEt_2)_2M'(PPh_3)$, **3c–f**, is obtained. Ligand redistribution again prevented the isolation of complexes **3**, and as a result the heterotrimetallic 2:1 adducts, **2i,j**, were characterized spectroscopically in the presence of the symmetric 2:1 products, **2e–h**. With the bulkier ligands, $Cp_2M(PR_2)_2$ (R = Ph, Cy), formation of the 2:1 complexes is precluded, and reaction with equimolar amounts of $CpPd(\eta\text{-}2\text{-}Me\text{-}allyl)$ or $Pt(1,5\text{-}COD)_2$ and PPh_3 affords the 1:1 monophosphine complexes, **3g–n** (Scheme II). Using $Cp_2M(PPh_2)_2$, this synthetic route was applied to a variety of phosphine and phosphite ligands, PX_3 (X = Me, Cy, OMe, O-*o*-tol), yielding the 1:1 monoligand complexes, **3o–v**. For M = Pd, L = $P(OMe)_3$, both mono- and bis(phosphite) complexes were observed by ^{31}P NMR spectroscopy at −98 °C; intermolecular phosphite exchange is fast at 25 °C. The stable bis(phosphine) complexes, $Cp_2M(\mu\text{-}PPh_2)_2M'(DMPE)$ (M = Hf, M' = Pd, **1g**; M = Zr, M' = Pt, **1h**), were obtained by DMPE substitution for PPh_3 in complexes **3l,m**.

Spectroscopic Characterization. Complexes **1–3** are yellow to red-orange crystalline solids and have been characterized by full elemental analyses and IR and ^1H and ^{31}P NMR spectroscopy. In addition, one member of each structural class has been characterized by single-crystal X-ray diffraction. The ^1H NMR spectra of complexes **1–3** all contain a cyclopentadienyl resonance between δ 5 and 6; in some cases a triplet splitting ($^3J_{P\text{-}H}$ = 1–1.5 Hz) is observed as found previously[4a] for $Cp_2M(PR_2)_2$ (M = Zr, Hf). The ^{31}P NMR spectra of complexes **1–3** all contain resonances at 80–150 ppm due to the bridging $(PR_2)^-$ ligands, in accord with those seen in analogous complex-

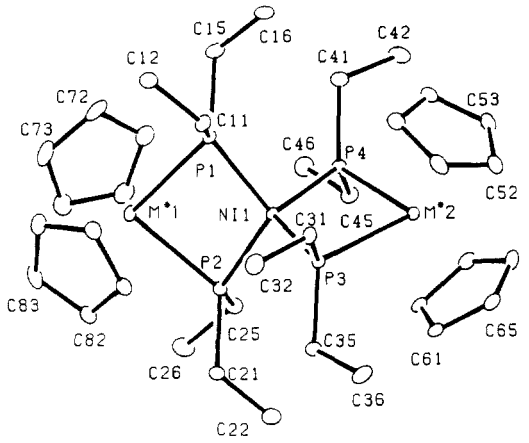

Figure 1. Molecular structure of $Cp_2Zr(\mu\text{-}PEt_2)_2Ni(\mu\text{-}PEt_2)_2HfCp_2$ (**2c**). Hydrogen atoms are omitted for clarity.

es.[7,18-20] In the 2:1 complexes, **2e–h**, the PR_2 bridge chemical shift difference is small going from Zr to Hf and large going from Pd to Pt, whereas the opposite is true for the 1:1 monophosphine complexes, **3c–n**. Coupling of the tertiary phosphorus ligands to the bridging $(PR_2)^-$ ligands varies from <1 to 30 Hz. More informative are the one-bond ^{195}Pt–P coupling constants. The Pt–PR_2 coupling decreases from R = Ph to Et to Cy and from M = Zr to Hf. For the 2:1 complexes, J_{Pt-P} = 2006 (1984) Hz for M = Zr (Hf); for the 1:1 bis(phosphine) complex, J_{Pt-P} = 2571 Hz for the PPh_2 bridge and 2879 Hz for the DMPE ligand. The 1:1 monoligand complexes show a much greater coupling to the phosphine ligand than to the phosphide bridge (cf. 3987 vs 2677 Hz for **3m**) and a greater dependence on the nature of the early metal (cf. J_{Pt-P} is ca. 60–70 Hz greater for the Zr analogues than for Hf, even for Pt–PR_3 coupling). Moreover, these values are small when compared, for example, with J_{Pt-P} = 4188 Hz for $Pt(PEt_3)_3$ and 3723 Hz for $Pt(PEt_3)_4$[21] and may result from expansion of the Pt coordination sphere or reduction of electron density on Pt, both resulting from interaction with the 16e⁻ group 4 metal center.

While the puckered ring observed for the DMPE complexes **1f–h** in the solid state renders the DMPE P's inequivalent, a single, sharp ^{31}P NMR resonance is observed for the DMPE ligands in all three complexes, even at −100 °C, indicating a low barrier to MP_2M' ring inversion.

The infrared spectra of the analogous complexes **3k–n** allow assignment of the Zr[Hf]–P (347 [302] cm^{-1}) and the Pd[Pt]–P (362 [377] cm^{-1}) stretching vibrations.[22]

Molecular Structures of $Cp_2Zr(\mu\text{-}PEt_2)_2Ni(\mu\text{-}PEt_2)_2HfCp_2$ (2c) and $Cp_2Hf(\mu\text{-}PPh_2)_2PdL$ (L = DMPE (1g), PPh_3 (3l)). The molecular structure of heterotrimetallic $Cp_2Zr(\mu\text{-}PEt_2)_2Ni(\mu\text{-}PEt_2)_2HfCp_2$, **2c**, shown in Figure 1, consists of 16e⁻ d^0 Cp_2Zr and -Hf moieties, each connected to a pseudotetrahedral 18e⁻ d^{10} Ni center via two $(PEt_2)^-$ bridges. While the ^{31}P NMR spectrum of isolated **2c** confirmed the absence of the Zr_2Ni or Hf_2Ni analogues, the Zr and Hf atoms are disordered with respect to their crystallographic positions and were refined with 50:50 occupancy. The MP_2Ni rings are nearly planar, and

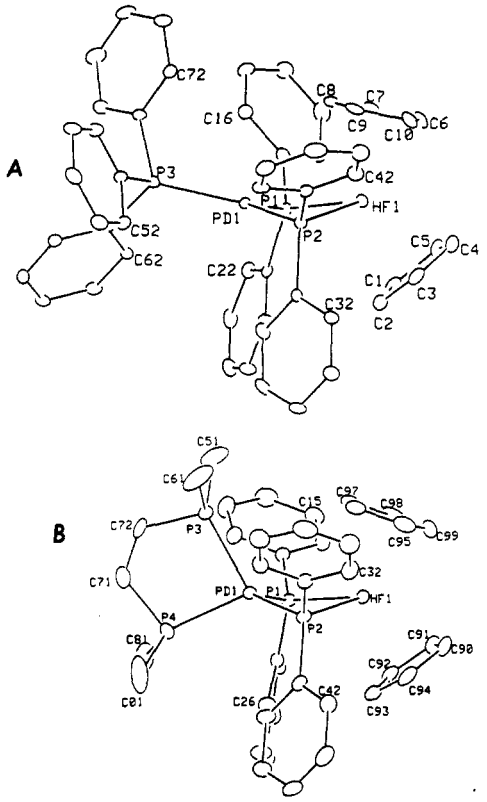

Figure 2. Molecular structures of (A) $Cp_2Hf(\mu\text{-}PPh_2)_2Pd(PPh_3)$ (**3l**) and (B) $Cp_2Hf(\mu\text{-}PPh_2)_2Pd(DMPE)$ (**1g**). Hydrogen atoms are omitted for clarity.

the average M···Ni distance is 3.027 (1) Å. The Hf–P bond distances and the angles about Hf and P are similar to those reported[7] for $Cp_2Hf(\mu\text{-}PEt_2)_2Mo(CO)_4$.

The molecular structures of $Cp_2Hf(\mu\text{-}PPh_2)_2PdL$ (L = DMPE, **1g**; PPh_3, **3l**), shown in Figure 2, consist of a 16e⁻ d^0 Cp_2Hf moiety connected to a pseudotetrahedral 18e⁻ d^{10} or a trigonal planar 16e⁻ d^{10} Pd center via two $(PPh_2)^-$ bridges with Hf···Pd distances of 2.983 (1) and 2.896 (1) Å, respectively. Both molecules have puckered HfP_2Pd rings, and coordination about Hf and P is compared to that found in similar bis$(PPh_2)^-$ bridged molecules in Table VII.

Reactivity Studies. No reaction was observed between the unsaturated Hf–Pd and Zr–Pt complexes, **3l,m**, and CO, H_2, or ethylene (1 atm, 25 °C) or with excess $CNBu^t$, benzaldehyde, or paraformaldehyde. Oxidative addition of MeI, a facile reaction with $Pt(PPh_3)_3$,[23] also does not occur with **3l,m** as noted by Gelmini and Stephan,[10] who found that acetylene complexes, $Cp_2Zr(\mu\text{-}PPh_2)_2Pt(PhC{\equiv}CH)$, could be formed by trapping the displaced PPh_3 with MeI. Protonation of the DMPE complexes, **1f–h**, with NH_4PF_6 led initially to the formation of M–H bonds (M = group 10 metal) as evidenced by ^1H NMR, but the resulting products were unstable with respect to bridge elimination reactions, which gave M–PPh_2H moieties. More reactive oxidative addends such as acetyl bromide also reacted with **3l,m** with disruption of the $(PPh_2)^-$ bridge.

EHMO Studies of the Early–Late Metal–Metal Bond in Bis$(PR_2)^-$-Bridged Heterobimetallics. To understand the bonding in **1–3** and related bis$(PR_2)^-$-bridged early–late heterobimetallics, we carried out molecular orbital calculations of the extended Hückel type[24] on a series of model complexes of the general formula

(18) Baker, R. T.; Tulip, T. H. *Organometallics* **1986**, *5*, 839.
(19) Gelmini, L.; Stephan, D. W. *Organometallics* **1988**, *7*, 849.
(20) Carty, A. J.; MacLaughlin, S. A.; Nucciarone, D. Stereochemistry of Metal Complexes: Phosphido Bridging Ligands. In *P-31 NMR Spectroscopy in Stereochemical Analysis*; Verkade, J. G., Quin, L. D., Eds.; VCH: Deerfield Beach, FL, 1987.
(21) Gerlach, D. H.; Kane, A. R.; Parshall, G. W.; Jesson, J. P.; Muetterties, E. L. *J. Am. Chem. Soc.* **1971**, *93*, 3453.
(22) Ferraro, J. R. *Low-Frequency Vibrations of Inorganic and Coordination Compounds*; Plenum Press: New York, 1971; pp 257–261.
(23) Belluco, U. *Organometallic and Coordination Chemistry of Platinum*; Academic Press: New York, 1974; p 222.

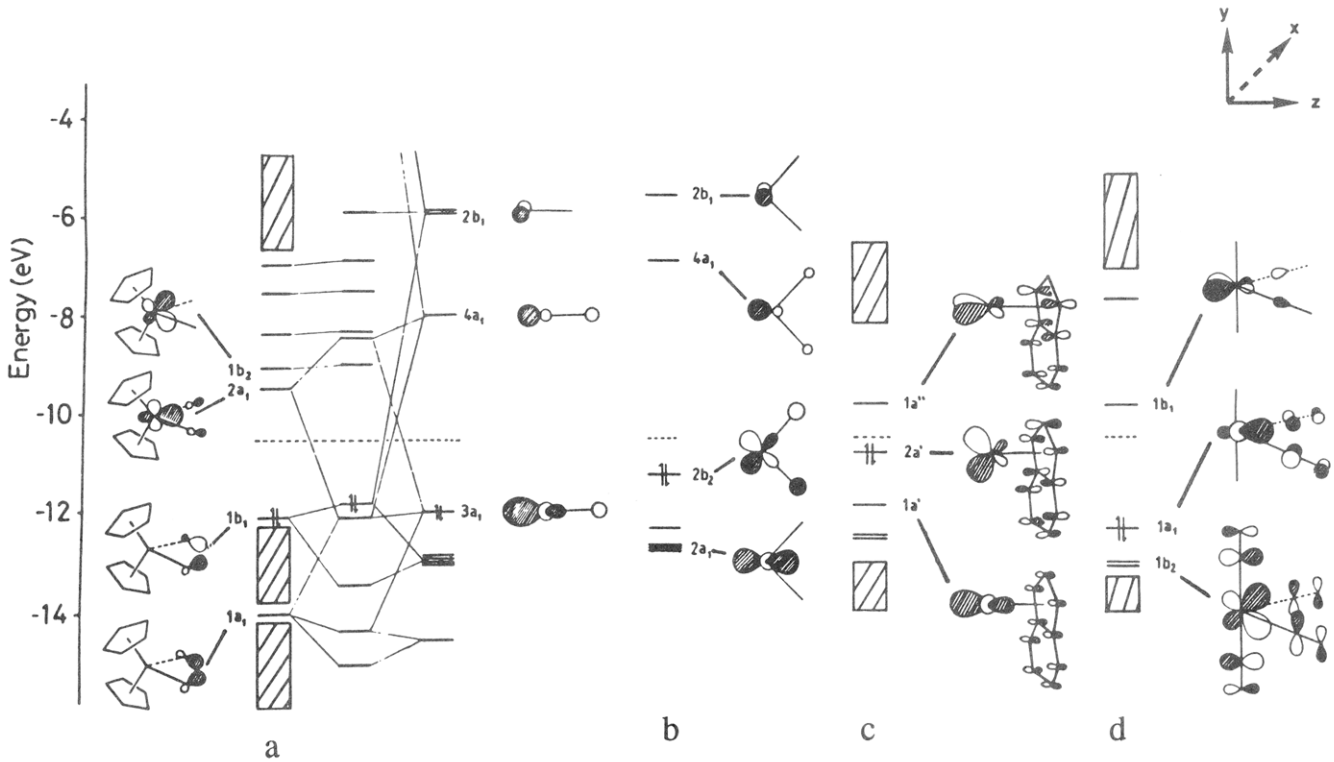

Figure 3. (a) Orbital interaction diagram for $Cp_2Zr(\mu\text{-}PH_2)_2PtL$ (**1''**). (b) Frontier orbitals for the $[PtL_2]$ fragment. (c) Frontier orbitals for the [Rh(η-indenyl)] fragment. (d) Frontier orbitals for the $[Mo(CO)_4]$ fragment.

$Cp_2Zr(\mu\text{-}PH_2)_2M'L_n$, where $M'L_n$ is Pt(DMPE), **1'**, Ni(μ-$PH_2)_2ZrCp_2$, **2'**, $Pt(PH_3)$, **3'**, Rh(η-indenyl), **4'**, and Mo(C-$O)_4$, **5'**. Geometries of the model compounds were derived from X-ray crystal structures with symmetrization and replacement of P-alkyl and -aryl groups by P–H (d_{P-H} = 1.42 Å). For **1'** and **3'**, further simplified models **1''** and **3''** were constructed in which the terminal phosphines were replaced by generalized two-electron-donor ligands L (Hückel parameters as for H). We also investigated the puckering[25] of the ZrP_2Pt ring in **1'** and **3'** by varying the dihedral angle (ϕ) between the ZrP_2 and PtP_2 planes.

It is pertinent to summarize the findings of two recent bonding analyses[26] on analogous actinide complexes. Hay et al. examined[26a] the bonding in (η-$C_5Me_5)_2Th(\mu$-$PPh_2)_2Pt(PMe_3)$, **6**, (Th···Pt = 2.984 Å) by carrying out ab initio calculations on the model compound $Cl_2Th(\mu$-$PH_2)_2Pt(PH_3)$, **6'**. Similarly Ortiz[26b] described the bonding in (η-$C_5Me_5)_2Th(\mu$-$PPh_2)_2Ni(CO)_2$,[27] **7**, (Th···Ni = 3.206 Å) by EHMO analysis on $Cp_2Th(\mu\text{-}PH_2)_2Ni(CO)_2$, **7'**. In each case, the analysis was prompted by interest in the nature and extent of the actinide–transition metal interaction. Hay et al. found that there was considerable M···M' interaction in **6'** of σ symmetry. This was derived mostly from the HOMO which was composed of an in-phase combination of Pt 5d(x^2–y^2) and Th 6d(x^2–y^2), where x is coincident with the Th–Pt vector. Ortiz found the actinide–transition metal interaction in **7'** to be much weaker. Bonding interactions of σ and π_y symmetries were found however.

Bonding between the $[M'L_n]$ and $[Cp_2Th(PH_2)_2]$ fragments is via lone-pair donation from the bridging phosphido groups to the late transition metal, with a weak secondary interaction of σ symmetry comprising back-donation from the late transition metal to empty low lying orbitals on thorium. In addition, the puckered ThP_2Pt ring observed for **6** afforded no *electronic* stabilization, as calculations indicated the planar form of **6'** to be 2.0 kcal mol^{-1} *more stable* than the puckered form. The results we present here are in qualitative agreement with these studies.

$[(Cp)_2Zr(PH_2)_2]$ Fragment. The frontier orbitals of the C_{2v} $[Cp_2Zr(PH_2)_2]$ fragment are shown on the left of Figure 3. The HOMO ($1b_1$) is largely ligand based. It is an out-of-phase combination of phosphorus sp(x)p(z) hybrids that are set up for interaction with a π_x acceptor orbital on $M'L_n$. The corresponding in-phase combination ($1a_1$) will be stabilized by interaction with an empty σ-orbital on $M'L_n$. The ability of $[Cp_2Zr(PH_2)_2]$ to function as a bis(phosphine) ligand can be traced to these two filled orbitals.

The Zr is formally in oxidation state IV and thus has a d^0 configuration. The five lowest lying virtual orbitals of the fragment constitute the empty Zr 4d block. The LUMO ($2a_1$) is set up to be a σ-acceptor orbital, which will play an important role in bonding to the late metal fragments. It is 62% localized on Zr, with s, p(z), d(x^2–y^2), and d(z^2) components. There are also empty Zr-based π-acceptor orbitals of π_x (b_1) and π_y (b_2) symmetries, which are of secondary importance compared with $2a_1$ because they

(24) (a) Hoffmann, R. *J. Chem. Phys.* **1963**, *39*, 1397. (b) Hoffmann, R.; Lipscomb, W. N.; *Ibid.* **1962**, *36*, 2179. (c) Hoffmann, R.; Lipscomb, W. N. *Ibid.* **1962**, *37*, 2872. (d) Parameters for the calculations were taken from ref 24e,f. For internal consistency, H*ii*'s for Zr were those used for W in ref 24f. All calculations were carried out using ICON8, with fragment MO analysis: Rossi, A.; Howell, J.; Wallace, D.; Haraki, K.; Hoffmann, R. Program ICON8, *QCPE No. 517*, **1986**, *6*, 100. Hückel constant = 1.75, and weighted H*ij* (modified Helmholz–Wolfsberg formula) were used throughout: Ammeter, J. H.; Burgi, H.-B.; Thibeault, J. C.; Hoffmann, R. *J. Am. Chem. Soc.* **1978**, *100*, 3686. (e) Summerville, R. H.; Hoffmann, R. *Ibid.* **1976**, *98*, 7240. (f) Dedieu, A.; Albright, T. A.; Hoffmann, R. *Ibid.* **1979**, *101*, 3141. (g) For early–late metal–metal bonds with substantial overlap populations see: Ferguson, G. S.; Wolczanski, P. T.; Parkanyi, L.; Zonnevylle, M. C. *Organometallics* **1988**, *7*, 1967.

(25) Pinhas, A. R.; Hoffmann, R. *Inorg. Chem.* **1979**, *18*, 654.

(26) (a) Hay, P. J.; Ryan, R. R.; Salazar, K. V.; Wrobleski, D. A.; Sattelberger, A. P. *J. Am. Chem. Soc.* **1986**, *108*, 313. (b) Ortiz, J. V. *Ibid.* **1986**, *108*, 550.

(27) Ritchey, J. M.; Zozulin, A. J.; Wrobleski, D. A.; Ryan, R. R.; Wasserman, H. J.; Moody, D. C.; Paine, R. T. *J. Am. Chem. Soc.* **1985**, *107*, 501.

Table VIII. Summary of the Results of EHMO Calculations

compound	M–M′ dist, Å	ROP[a] (M–M′)	atomic charge[b] M	atomic charge[b] M′
3′, Pt (PH_3) (ϕ = 0)	2.967	0.106	+0.76	−0.82
3′, Pt (PH_3) (ϕ = 25.5°)	2.896	0.116	+0.76	−0.82
3″, Pt (L)	2.90	0.112	+0.83	−0.85
1″, Pt (L_2)	2.90	0.128	+0.78	−1.10
1″, Pt (L_2)[c]			−0.41	−0.25
4′, Rh (indenyl)	3.05	0.109	+0.61	−0.02
2′, Zr–Ni–Zr	3.05	0.048	+0.97	−1.40
5′, $Mo(CO)_4$	3.35	0.060	+0.80	−0.20

[a] ROP = reduced overlap population. [b] M = Zr; M′ = late metal (Pt, Rh, Ni, Mo). [c] Platinum in square-planar rather than tetrahedral geometry.

are higher in energy and not as well-directed, so that orbital overlap with the late metal will be poorer.

$Cp_2Zr(\mu\text{-}PH_2)_2Pt(PH_3)$ (3′). The M···M′ internuclear separation of 2.896 (1) Å observed in $Cp_2Hf(\mu\text{-}PPh_2)_2Pd(PPh_3)$ is the shortest in the series, and if appreciable M···M′ interactions are present in these compounds, they should certainly be in evidence for 3′. A key feature is the Zr/Pt reduced overlap population (ROP) of 0.116, indicating a net bonding relationship between the metals, in contrast with Ortiz' findings[26b] for the Th/Ni compound 7′. Although the degree of M···M′ bonding cannot be quantified with accuracy by the EHMO technique, the M/M′ ROPs in compounds 1′–5′ provide a qualitative indication of the degree of M···M′ interaction as a function of geometry and the $M'L_n$ fragment (Table VIII).

In 3′ there are only minor changes in the bonding as the dihedral angle (ϕ) is reduced to 0.0° to attain a planar ZrP_2Pt ring. The total energy for 3′ in the planar geometry is only 0.20 eV higher than that for the puckered form based on its solid-state structure (ϕ = 25.5°). This puts an upper limit of ca. 5 kcal mol^{-1} on the barrier to interconversion of the phosphido substituents. This value is probably overestimated due to the crude way in which the planar form was derived. The decrease in the Zr/Pt ROP to 0.106 may be attributed to the fact that the Zr···Pt distance has been increased to 2.967 Å in the planar form.

The bonding in 3″ is shown in Figure 3. The [$Pt(PH_3)$] fragment was replaced by [PtL], with ϕ = 0°, to preserve molecular C_{2v} symmetry. The orbitals of the [PtL] fragment are shown in Figure 3b. The important interactions between the two fragments are of a_1 (σ) and b_1 (π_x) symmetry. Out-of-plane b_2 (π_y) interactions may be identified (cf. the findings of Ortiz[26b]) but are essentially net nonbonding in this instance. The ($1b_1$) HOMO of the Zr fragment interacts with empty Pt p(x) and filled Pt d(xz), to form a Pt–μ-P bonding combination, pushing the orbital that is principally Pt d(xz) up in energy to become the *molecular* HOMO. Mixing of Zr ($2b_1$) with this latter orbital leads to overall stabilization of the filled b_1 levels. Formally, the other Pt–μ-P bonding orbital comes from the interaction of the in-phase P sp(x)p(z) hybrid ($1a_1$ of the Zr fragment) with the Pt sp(z) LUMO ($4a_1$). These are well separated in energy, so that stabilization of the former by the latter is indirect.

The key interaction between the metals is via $2a_1$ of the Zr fragment and $3a_1$ of [PtL]. The M/M′ ROP stems *almost* entirely from the overlap of the metal z and z^2 orbitals, which occurs on mixing of the Zr-based LUMO with the HOMO of the Pt fragment. The Pt → Zr donor–acceptor σ-bond is polarized toward the late metal (57% Pt, 22% Zr). This interaction can be seen as relieving the charge buildup on the Pt atom caused by donation from the phosphido bridges. The fragment and atomic charges provide support for this model. Both metal centers are more negatively charged in the molecule than in their respective fragments, with the electron density coming from the bridging phosphorus atoms. The net charge transfer to the Pt fragment is due to donation from the μ-P atoms to Pt with *lesser* back-donation from the Pt atom to Zr.

$Cp_2Zr(\mu\text{-}PH_2)_2Pt(DMPE)$ (1′). The model compound 1′ is based on the crystal structure of the Hf–Pd analogue, **1g**, with Hf···Pd = 2.983 (1) Å, slightly longer than in **3l**; there is also a similar degree of puckering (ϕ = 27.2°).

Many of the features resemble those of 3′. The Zr–Pt ROP (0.123 for ϕ = 27.2°) is similar to that in 3′, in spite of the larger internuclear separation. Again, as ϕ is lowered, the ROP decreases and the total energy of the molecule is raised. The frontier orbitals of the [PtL_2] fragment in 1″ are shown in Figure 3b. As in 3″, Pt d(z^2) is destabilized by mixing with filled ligand σ-orbitals. In[PtL_2], the two ligands are not directed along z, so the overall destabilization of d(z^2) is *less* than that caused by the single axial ligand in [PtL]. As a result, the [PtL] fragment in 3″ is a better σ-donor to Zr than [PtL_2] in 1″, even though [PtL_2] is more electron rich than [PtL]. The [PtL_2] HOMO ($2b_2$) is relatively high in energy and interacts with the empty Zr-based $2b_2$ orbital, leading to a small π_y contribution to the M/M′ ROP.

We have also analyzed the effect of varying the orientation of the ligands in 1″. If the [PtL_2] fragment is rotated by 90°, so that the Pt is square-planar, the compound is destabilized by 2.8 eV. In this orientation, the complex is forced to be formally Zr(II)–Pt(II). The HOMO is at −8.4 eV, well separated from the other filled levels and only 0.4 eV below the LUMO. If two electrons are removed from 1″, however, the square-planar geometry is favored over the pseudotetrahedral geometry by 1.5 eV. Electrochemical studies on **1d–f** are in progress to verify these conclusions, and the related d^8 [ML_2] complex $[Cp_2Zr(\mu\text{-}PEt_2)_2Rh(DMPE)]^+$ has recently been prepared.[28]

$Cp_2Zr(\mu\text{-}PH_2)Rh(\eta^5\text{-indenyl})$ (4′). This complex is a model for $Cp_2Zr(\mu\text{-}PPh_2)_2Rh(\eta^5\text{-indenyl})$ (**4**), which has crystallographic C_s symmetry[18] with the mirror plane orthogonal to the nearly planar ZrP_2Rh ring. The frontier orbitals for the d^8 [$M'L_3$] [Rh(indenyl)] fragment are shown in Figure 3c. The bonding in 4′ is qualitatively similar to that in 1″. The Zr/Rh ROP (0.109) is again principally due to σ-interactions with a small π_y contribution.

In solution, **4** exhibits hindered rotation[18,29] of the indenyl ring with $\Delta G^{\ddagger}$ of 14.0 ± 0.3 kcal mol^{-1}. We have examined the effect of rotating the indenyl ring in the xy plane. The π-bonding between the fragments in 4′ is optimized when the Zr HOMO $1b_1$ interacts with the Rh LUMO 1a″, and the Rh HOMO 2a′ interacts with empty Zr $1b_2$. The conformation observed in the solid state, with the long axis of the indenyl along y, is found to be 0.37 eV (ca. 9.0 kcal mol^{-1}) more stable than when the indenyl lies along x. The preferred orientation in 4′ is consistent with that observed for all (indenyl)RhL_2 complexes where the two ligands, L, straddle the molecular mirror plane.[29] This preference can be traced to the nondegeneracy of the two highest filled π orbitals of the indenyl ligand.

(28) Baker, R. T., unpublished results.

(29) (a) Barr, R. D.; Green, M.; Marder, T. B.; Stone, F. G. A. *J. Chem. Soc., Dalton Trans.* **1984**, 1261. (b) Marder, T. B.; Calabrese, J. C.; Roe, D. C.; Tulip, T. H. *Organometallics* **1987**, *6*, 2012. (c) Carl, R. T.; Hughes, R. P.; Rheingold, A. L.; Marder, T. B.; Taylor, N. J. *Ibid.* **1988**, *7*, 1613. (d) Kakkar, A. K.; Jones, S. F.; Taylor, N. J.; Collins, S.; Marder, T. B. *J. Chem. Soc., Chem. Commun.* **1989**, 1454. (e) Kakkar, A. K.; Taylor, N. J.; Calabrese, J. C.; Nugent, W. A.; Roe, D. C.; Connaway, E. A.; Marder, T. B. *Ibid.* **1989**, 990.

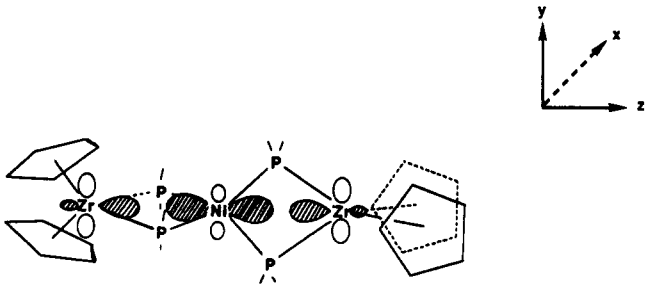

Figure 4. Three-center Zr···Ni···Zr bonding orbital in **2′**.

$Cp_2Zr(\mu\text{-}PH_2)_2Mo(CO)_4$ (5′). The synthesis and X-ray crystal structures of the compounds $Cp_2Hf(\mu\text{-}PEt_2)_2Mo(CO)_4$[7] and $Cp_2Zr(\mu\text{-}PPh_2)_2M(CO)_4$ (M = Mo,[30a] W[30b]) have been reported. They are isolobal analogues of the compounds **1′** and **4′** with a d^6 $[M'L_4]$ fragment attached to the early metal rather than d^{10} $[M'L_2]$ or d^8 $[M'L_3]$. These compounds display much larger M···M′ separations (3.400 (1), 3.299 (1), and 3.289 (1) Å, respectively) than the platinum and rhodium complexes discussed above. The frontier orbitals of the C_{2v} $[Mo(CO)_4]$ fragment[31] are shown in Figure 3d. The fragment HOMO $1a_1$, the σ-donor orbital, is predominantly $d(x^2-y^2)$ and $d(z^2)$; however, mixing in of metal s and $p(z)$ enhances π-back-bonding interactions with the two CO ligands in the xz plane and spatially contracts the orbital lobe directed toward Zr $2a_1$. Thus the M/M′ overlap is greatly reduced relative to **1′** and **3′** because M′ $p(z)$ is now making an antibonding rather than a bonding contribution. The π-acid ligands make the fragment a very poor σ-donor. The relatively weak Th–Ni interaction[26b] in **7** may also be attributed to this effect.

$[Cp_2Zr(\mu\text{-}PH_2)_2]_2Ni$ (2′). The analysis of **2′** differs from that of **1′** in the following ways that explain the effectively much longer M···M′ distance in **2c**. There are now two Zr centers that can accept electron density from the nickel. The lower orbital energies of Ni compared to Pt reduce the need for extensive bonding to the early metals and allow greater charge buildup on Ni. The net effect is that the M···M′ ROP is considerably smaller (0.048) than in **1′**. The main contributions to the Zr/Ni ROP are interaction of Ni $d(z^2)$ with an in-phase combination of Zr fragment a_1 orbitals, and Ni $p(z)$ with an out-of-phase combination of Zr a_1 orbitals (Figure 4).

Our bonding analysis for both **2′** and **5′** can also be applied to analogous compounds in which the phosphido bridges are replaced by (μ-SR) groups.[32]

Conclusion

We have demonstrated the binding of d^{10} $[M'L_2]$, $[M'L]$, and $[M']$ fragments to the metal-containing bis(phosphines), $Cp_2M(PR_2)_2$ (M = Zr, Hf; R = Et, Ph, Cy). The $Cp_2M(\mu\text{-}PR_2)_2M'L_n$ (n = 1, 2) complexes exhibit puckered $M(\mu\text{-}PR_2)_2M'$ rings in the solid state, whereas the $\{Cp_2M(\mu\text{-}PR_2)_2\}_2M'$ species have nearly planar $M(\mu\text{-}PR_2)_2M'$ cores. EHMO calculations indicate very little energy difference between planar and puckered $M(\mu\text{-}PR_2)_2M'$ rings. Consistent with this observation is the fact that the solution NMR studies indicate equivalence of the $(\mu\text{-}PR_2)^-$ substituents even at very low temperatures. An alternative geometry for the $Cp_2M(\mu\text{-}PR_2)_2M'L_2$ complexes, in which the M′ center is square-planar rather than pseudotetrahedral, was found to be greatly destabilized for M′ = d^{10} but stabilized for M′ = d^8. For the d^{10} case, this clearly demonstrates that the complexes should be regarded as M(IV)–M′(0) rather than M(II)–M′(II) species. For the previously reported[18] complexes of the form $[Cp_2M(\mu\text{-}PR_2)_2Rh(\eta\text{-indenyl})]$, we also analyzed the rotational preference of the indenyl ring. The complex was found to be ca. 9 kcal mol^{-1} more stable when the two (μ-PR_2) groups straddle the mirror plane of the Rh(η-indenyl) group, consistent with the solid-state structure and the observed barriers to hindered indenyl ring rotation of ca. 14 kcal mol^{-1}.

Finally, the relative strength of the M′ → M donor–acceptor bonds in $Cp_2M(\mu\text{-}PR_2)_2M'L_n$ complexes depends strongly on the nature of the $M'L_n$ fragment. $Mo(CO)_4$ was found to be a poor σ-donor, particularly due to the rehybridization of the σ-orbitals caused by back-bonding to CO. On the other hand, $Pt(PR_3)$ is an excellent σ-donor because Pt $d(z^2)$ is strongly *destabilized* by the PR_3 group. The M′ → M donor–acceptor interactions effectively reduce electron density on M′, resulting in a significantly diminished tendency to undergo oxidative addition reactions.

Acknowledgment. We are indebted to S. A. Hill, L. F. Lardear, J. D. Center, G. Watunya, and E. A. Conaway for their fine technical assistance, J. V. Ortiz for communication of results prior to publication, D. M. P. Mingos, R. L. Johnston, and J.-F. Halet for valuable discussions, and J. C. Calabrese for assistance with the crystallography. T.B.M. is grateful to the University of Waterloo, the Natural Sciences and Engineering Research Council of Canada, and the donors of the Petroleum Research Fund, administered by the American Chemical Society, for financial support.

Registry No. **1a**, 127518-03-0; **1b**, 127518-04-1; **1c**, 127518-05-2; **1d**, 127518-06-3; **1e**, 127518-07-4; **1f**, 127518-08-5; **1g**, 127518-09-6; **1h**, 127518-10-9; **1i**, 127518-11-0; **2a**, 127518-12-1; **2b**, 127540-27-6; **2c**, 127518-13-2; **2c**·$^1/_2$THF, 127518-14-3; **2d**, 127518-21-2; **2e**, 127518-15-4; **2f**, 127518-16-5; **2g**, 127518-17-6; **2h**, 127518-18-7; **2i**, 127518-19-8; **2j**, 127518-20-1; **2′**, 127518-43-8; **3a**, 127540-28-7; **3b**, 127518-22-3; **3c**, 127518-23-4; **3d**, 127518-24-5; **3e**, 127518-25-6; **3f**, 127518-26-7; **3g**, 127518-27-8; **3h**, 127518-28-9; **3i**, 127518-29-0; **3j**, 127518-30-3; **3k**, 100946-11-0; **3l**, 127518-31-4; **3m**, 100946-12-1; **3n**, 127518-32-5; **3o**, 127518-33-6; **3p**, 127518-34-7; **3q**, 127518-35-8; **3r**, 127518-36-9; **3s**, 127518-37-0; **3t**, 127518-38-1; **3u**, 127518-39-2; **3v**, 127518-40-5; **3′**, 127518-42-7; **4′**, 127540-29-8; **5′**, 127518-44-9; $Cp_2Zr(PEt_2)_2$, 86013-23-2; $Ni(1,5\text{-}COD)_2$, 1295-35-8; $Cp_2Hf(PEt_2)_2$, 86013-26-5; $Cp_2Hf[PhP(CH_2)_3PPh]$, 127518-41-6; $Pd(PPh_3)_4$, 14221-01-3; CpPd(2-Me-allyl), 33593-95-2; $Pt(PPh_3)_3$, 28516-49-6; $Cp_2Zr(PCy_2)_2$, 86013-24-3; $Cp_2Hf(PCy_2)_2$, 86013-27-6; $Cp_2Zr(PPh_2)_2$, 86013-25-4; $Cp_2Hf(PPh_2)_2$, 86013-28-7; $Pt(1,5\text{-}COD)_2$, 12130-66-4.

Supplementary Material Available: Tables of complete elemental analytical data (C, H, P, M, M′) and IR spectroscopic data for all listed complexes and tables of final positional and thermal parameters for the non-hydrogen atoms, fixed hydrogen atom coordinates, and anisotropic thermal parameters for complexes **1g**, **2c**, and **3l** (16 pages); listings of observed and calculated structure factor amplitudes (45 pages). Ordering information is given on any current masthead page.

(30) (a) Gelmini, L.; Matassa, L. C.; Stephan, D. W. *Inorg. Chem.* **1985**, *24*, 2585. (b) Targos, T. S.; Rosen, R. P.; Whittle, R. R.; Geoffroy, G. L. *Ibid.* **1985**, *24*, 1375.

(31) The $M(CO)_4$ fragment has been discussed previously: (a) Elian, M.; Hoffmann, R. *Inorg. Chem.* **1975**, *14*, 1058. (b) Hofmann, P. *Angew. Chem.* **1979**, *91*, 951.

(32) (a) Cameron, T. S.; Prout, C. K.; Rees, G. V.; Green, M. L. H.; Joshi, K. K.; Davies, G. R.; Kilbourn, B. T.; Braterman, P. S.; Wilson, V. A. *J. Chem. Soc., Chem. Commun.* **1971**, 14. (b) Douglas, W. E.; Green, M. L. H.; Prout, C. K.; Rees, G. V. *Ibid.* **1971**, 896.